Probabilistic Engineering Mechanics 29 (2012) 176–188

Contents lists available at SciVerse ScienceDirect

Probabilistic Engineering Mechanics

journal homepage: www.elsevier.com/locate/probengmech

A reliability-based framework for fatigue damage prognosis of composite aircraft structures

Maurizio Gobbato [a], Joel P. Conte [a,*], John B. Kosmatka [a], Charles R. Farrar [b]

[a] Department of Structural Engineering, University of California, San Diego, 9500 Gilman Dr., La Jolla, CA 92093-0085, United States
[b] The Engineering Institute, MS T-001, Los Alamos National Laboratory, Los Alamos, NM 87545, United States

ARTICLE INFO

Article history:
Received 5 November 2010
Received in revised form
3 November 2011
Accepted 17 November 2011
Available online 2 December 2011

keywords:
Fatigue damage prognosis
Structural health monitoring
Probabilistic damage detection
Damage evolution
System reliability
Composite unmanned aerial vehicles

ABSTRACT

The extensive use of lightweight composite materials in composite aircraft structures drastically increases the sensitivity to both fatigue- and impact-induced damage of their critical structural components during their service life. Within this scenario, an integrated hardware–software system that is capable of monitoring the composite airframe, assessing its structural integrity, identifying a condition-based maintenance, and predicting the remaining service life of its critical components is therefore needed. As a contribution to this goal, this paper presents the theoretical basis of a novel and comprehensive probabilistic methodology for predicting the remaining service life of adhesively bonded joints within the structural components of composite aircraft, with emphasis on a composite wing structure. Non-destructive evaluation techniques and recursive Bayesian inference are used to (i) assess the current state of damage of the system and (ii) update the joint probability distribution function (PDF) of the damage extents at various locations. A probabilistic model for future aerodynamic loads and a damage evolution model for the adhesive are then used to stochastically propagate damage through the joints and predict the joint PDF of the damage extents at future times. This information is subsequently used to probabilistically assess the reduced (due to damage) global aeroelastic performance of the wing by computing the PDFs of its flutter velocity and the velocities associated with the limit cycle oscillations of interest. Combined local and global failure criteria are finally used to compute lower and upper bounds for the reliability index of the composite wing structure at future times.

1. Introduction

Probabilistic design, structural health monitoring (SHM), and risk assessment methodologies for commercial, transport, and fighter aircraft have been under development by the research community for a considerable time [1–3]. Moreover, the increasing use of high-performance lightweight composite materials is rendering rigorous probabilistic approaches essential: fiber-reinforced polymer (FRP) and adhesive materials are in fact characterized by a large statistical variability in their mechanical properties and are extremely sensitive to both fatigue- and impact-induced damage — phenomena that cannot be treated deterministically and require periodic monitoring of the structure in order to prevent unexpected failures. Unmanned aerial vehicles (UAVs), such as the one shown in Fig. 1, are an example of how extensively composite materials can be used in aircraft structures; additionally, the absence of a pilot on these vehicles leads to higher levels of damage tolerance. Various damage mechanisms — e.g., debonding, inter-ply delamination, fiber breakage, and matrix cracking — can thus initiate and invisibly propagate up to catastrophic levels in the most damage-sensitive structural components, such as the wings, the tail stabilizers, and the fuselage. In particular, the adhesive joints that bond the aircraft skin to the primary airframe components (e.g., wing spars, bulkheads, stringers) are recognized as the most fatigue-sensitive subcomponents of a lightweight composite aircraft, with the wing skin-to-spar adhesive joints being the most critical. The progressive debonding, evolving from the wing root along these joints (see Fig. 1 and [4]), compromises both local component strength and global aeroelastic performance of the vehicle [5,6]. There is therefore the need for a field-deployable system capable of monitoring the composite airframe, assessing its structural integrity, identifying a cost-efficient condition/risk-based maintenance program, and predicting its remaining useful life (damage prognosis; see [7]).

The probabilistic framework for remaining service life prediction presented in this paper was inspired by a performance-based analysis framework developed in the area of earthquake engineering [8]. According to this approach, data collected during on-ground and in-flight non-destructive evaluation (NDE) inspections [9] are used to assess the current state of damage of the monitored structural components (i.e., damage location, damage

* Corresponding author. Tel.: +1 858 822 4545; fax: +1 858 822 2260.
E-mail addresses: mgobbato@ucsd.edu (M. Gobbato), jpconte@ucsd.edu (J.P. Conte), jkosmatka@ucsd.edu (J.B. Kosmatka), farrar@lanl.gov (C.R. Farrar).

0266-8920/$ – see front matter
doi:10.1016/j.probengmech.2011.11.004

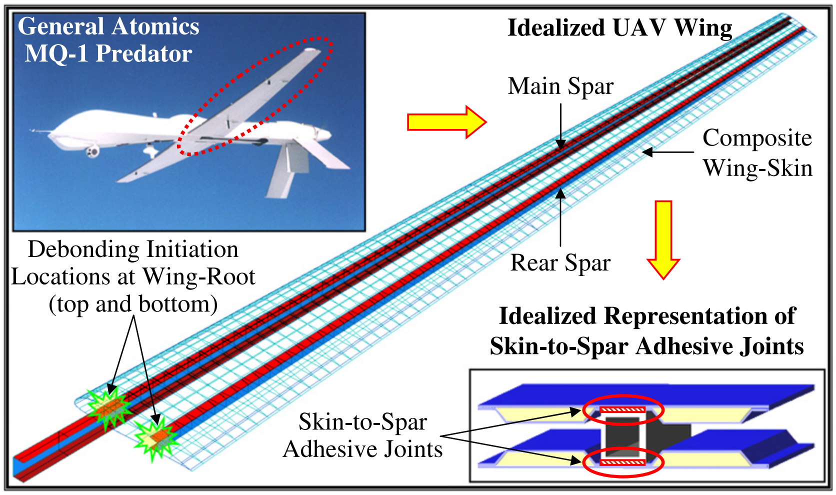

Fig. 1. Example of a composite UAV and idealized composite UAV wing with emphasis on the skin-to-spar adhesive joints and the four possible locations of damage initiation at the wing root.

mechanism, and damage size/extent) considering potential multiple damage mechanisms and locations. The uncertainty characterizing the NDE inspection results is efficiently assimilated by a recursive Bayesian inference scheme used to update the joint probability distribution function (PDF) of the damage extents. A load hazard model for future aerodynamic loads and a damage evolution model are then used to stochastically propagate the identified damage mechanisms in time. Finally, combined local (e.g., exceedance of a critical damage size at a damage location) and global (e.g., exceedance of the flutter instability boundary, or initiation of limit cycle oscillation (LCO) behavior) failure criteria, similar to those introduced by Lin et al. [10] and Styuart et al. [11], are used to compute the evolution in time of the probability of *system failure* using well-established component and system reliability analysis methods.

2. Overview of proposed damage prognosis methodology

The flowchart shown in Fig. 2 illustrates conceptually the process of uncertainty propagation necessary to estimate the remaining service life of a composite aircraft structural component (e.g., a composite UAV wing) once a new NDE inspection outcome, at current time t_p, becomes available. The inspection outcome is represented by the measured (through NDE sensor data processing) damage size/extent vector, $\mathbf{a}_m^p$, at the inspected locations at time t_p. This new information is used (in the first step of the methodology, *Bayesian inference*) to compute the posterior joint PDF of the (n_{A}^p-dimensional) actual damage size vector, $\mathbf{A}_a^p$, conditional on the material ($\boldsymbol{\Theta}_{\mathrm{mat}}$) and damage model ($\boldsymbol{\Theta}_{\mathrm{dam}}$) parameters, as well as on all the previous $p+1$ NDE measurement outcomes obtained up to time t_p, denoted as $\mathbf{a}_m^{[0,p]} = \left\{\mathbf{a}_m^0, \mathbf{a}_m^1, \ldots, \mathbf{a}_m^p\right\}$. For the sake of simplicity, this posterior joint conditional PDF, given in full form as $f''_{\mathbf{A}_a^p|\boldsymbol{\Theta}_{\mathrm{mat}},\boldsymbol{\Theta}_{\mathrm{dam}},\mathbf{A}_m^{[0,p]}}\left(\mathbf{a}_a^p\,|\boldsymbol{\theta}_{\mathrm{mat}}, \boldsymbol{\theta}_{\mathrm{dam}}, \mathbf{a}_m^{[0,p]}\right)$, is hereafter denoted $f''_{\mathbf{A}_a^p|\boldsymbol{\Theta}_{\mathrm{mat}},\boldsymbol{\Theta}_{\mathrm{dam}}}\left(\mathbf{a}_a^p\,|\boldsymbol{\theta}_{\mathrm{mat}}, \boldsymbol{\theta}_{\mathrm{dam}}\right)$, without explicitly including the dependency on $\mathbf{A}_m^{[0,p]}$. Similarly, the prior knowledge is denoted as $f'_{\mathbf{A}_a^p|\boldsymbol{\Theta}_{\mathrm{mat}},\boldsymbol{\Theta}_{\mathrm{dam}}}\left(\mathbf{a}_a^p\,|\boldsymbol{\theta}_{\mathrm{mat}}, \boldsymbol{\theta}_{\mathrm{dam}}\right)$. Furthermore, the actual size of the jth detected damage mechanism evolving at the ith monitored damage location at time t_p is denoted as $A_a^{(i,j,p)}$. The random parameter vector $\boldsymbol{\Theta}_{\mathrm{mat}}$ (of length n_{mat}) exclusively describes the uncertainty in the material properties used to model the parts of the airframe which are herein assumed to be non-damageable, while the random vector $\boldsymbol{\Theta}_{\mathrm{dam}}$ (of length n_{dam}) quantifies the uncertainty of those parameters that control the fatigue-induced material degradation [12–14] in the pre-identified damageable subcomponents. In this study, $\boldsymbol{\Theta}_{\mathrm{mat}}$ and $\boldsymbol{\Theta}_{\mathrm{dam}}$ are assumed to be statistically independent (s.i.) and time invariant [15].

The second step of the methodology, *probabilistic load hazard analysis*, defines the joint PDF of the s.i. [15] turbulence and maneuver intensity measures ($\mathbf{IM}_{\mathrm{T}}, \mathbf{IM}_{\mathrm{M}}$), conditional on the flight profile ($\boldsymbol{\Theta}_{\mathrm{F}}$) and the assumed s.i. turbulence ($\boldsymbol{\Theta}_{\mathrm{T}}$) and maneuver ($\boldsymbol{\Theta}_{\mathrm{M}}$) random parameter vectors; i.e., the joint conditional PDF $f_{\mathbf{IM}|\boldsymbol{\Theta}_{\mathrm{F}}}(\mathbf{im}\,|\boldsymbol{\theta}_{\mathrm{F}}) = f_{\mathbf{IM}_{\mathrm{T}},\mathbf{IM}_{\mathrm{M}}|\boldsymbol{\Theta}_{\mathrm{F}}}(\mathbf{im}_{\mathrm{T}}, \mathbf{im}_{\mathrm{M}}\,|\boldsymbol{\theta}_{\mathrm{F}})$. This step thus provides the information on the aerodynamic loads necessary to stochastically compute the structural response of interest at future time $t > t_p$. In the proposed methodology, this task is achieved in a discrete fashion [15] by defining $\bar{q}$ equally spaced future times $\left\{t_p^q = t_p + q\Delta\tau, q = 1, 2, \ldots, \bar{q}\right\}$. Within the time window $\left[t_p, t_p^{\bar{q}}\right]$ an unknown number of flight segments (n_s) can occur, and therefore $\boldsymbol{\Theta}_{\mathrm{F}}$ collects the flight profile parameters for each of these n_s flight segments as $\boldsymbol{\Theta}_{\mathrm{F}} = \left\{\boldsymbol{\Theta}_{\mathrm{F}}^{(k)}, k = 1, \ldots, n_s\right\}$. Examples of parameters collected in $\boldsymbol{\Theta}_{\mathrm{F}}^{(k)}$ include the altitude of flight, $H^{(k)}$; the mean airstream velocity with respect to (w.r.t.) a reference system fixed to the aircraft, $\mathbf{V}^{(k)}$; and the time of flight during the kth flight segment, $T^{(k)}$. Similarly, it is possible to rewrite the vectors $\mathbf{IM}_{\mathrm{T}}$, $\mathbf{IM}_{\mathrm{M}}$, $\boldsymbol{\Theta}_{\mathrm{T}}$, and $\boldsymbol{\Theta}_{\mathrm{M}}$ as $\mathbf{IM}_{\mathrm{T}} = \left\{\mathbf{IM}_{\mathrm{T}}^{(k)}, k = 1, \ldots, n_s\right\}$, $\mathbf{IM}_{\mathrm{M}} = \left\{\mathbf{IM}_{\mathrm{M}}^{(k)}, k = 1, \ldots, n_s\right\}$, $\boldsymbol{\Theta}_{\mathrm{T}} = \left\{\boldsymbol{\Theta}_{\mathrm{T}}^{(k)}, k = 1, \ldots, n_s\right\}$, and $\boldsymbol{\Theta}_{\mathrm{M}} = \left\{\boldsymbol{\Theta}_{\mathrm{M}}^{(k)}, k = 1, \ldots, n_s\right\}$, respectively. The n_s subvectors $\mathbf{IM}_{\mathrm{T}}^{(k)}$ are assumed to be mutually s.i. and independent of $\boldsymbol{\Theta}_{\mathrm{M}}$. Similarly, the n_s subvectors $\mathbf{IM}_{\mathrm{M}}^{(k)}$ are assumed to be mutually s.i. and independent of $\boldsymbol{\Theta}_{\mathrm{T}}$.

In the third step of the proposed methodology, namely *probabilistic structural response analysis*, the joint conditional PDF of the structural response of the system – expressed in terms of the predicted (from time t_p) damage size vector ($\mathbf{A}_a^{[p,q]}$) at the generic future time $t_p^q = t_p + q\Delta\tau$ with $q \in \{1, 2, \ldots, \bar{q}\}$ – is computed through extensive Monte Carlo (MC) simulations or semi-analytical methods using either the detailed finite element (FE) model of the structure or a computationally more efficient surrogate model [16]. This joint PDF, conditional on $\boldsymbol{\Theta}_{\mathrm{mat}}$, $\boldsymbol{\Theta}_{\mathrm{dam}}$, and all the previous NDE outcomes $\mathbf{a}_m^{[0,p]}$ (not explicitly included in the notation), is denoted $f_{\mathbf{A}_a^{[p,q]}|\boldsymbol{\Theta}_{\mathrm{mat}},\boldsymbol{\Theta}_{\mathrm{dam}}}\left(\mathbf{a}_a^{[p,q]}\,|\boldsymbol{\theta}_{\mathrm{mat}}, \boldsymbol{\theta}_{\mathrm{dam}}\right)$, and is computed as shown later in Eq. (3).

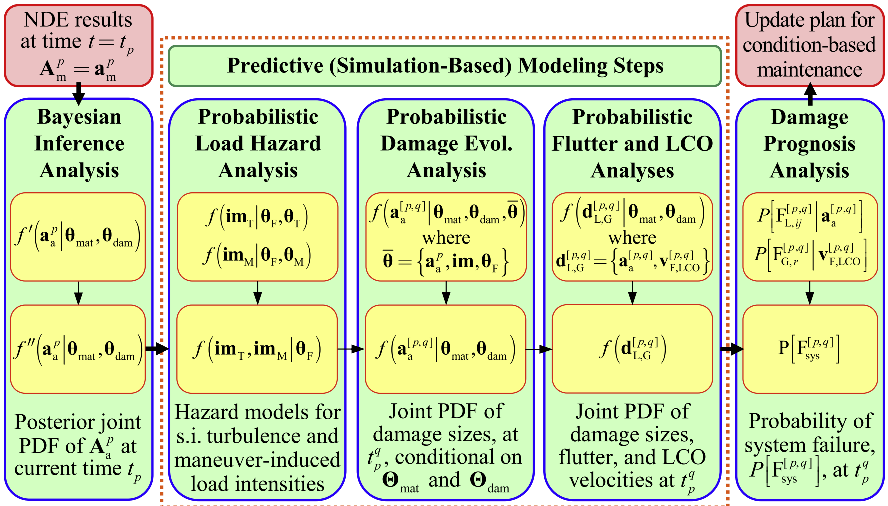

Fig. 2. Overview of proposed reliability-based damage prognosis methodology for remaining service life prediction.

The fourth step, namely *probabilistic flutter and LCO analyses*, estimates the joint PDF of the predicted damage size vector $\mathbf{A}_a^{[p,q]}$, flutter velocity $V_{\mathrm{F}}^{[p,q]}$, and the (n_{LCO}-dimensional) vector of LCO velocities ($\mathbf{V}_{\mathrm{LCO}}^{[p,q]}$) at the generic future time $t_p^q = t_p + q\Delta\tau$, i.e., the joint PDF $f_{\mathbf{A}_a^{[p,q]}, V_{\mathrm{F}}^{[p,q]}, \mathbf{V}_{\mathrm{LCO}}^{[p,q]}}\left(\mathbf{a}_a^{[p,q]}, v_{\mathrm{F}}^{[p,q]}, \mathbf{v}_{\mathrm{LCO}}^{[p,q]}\right) = f_{\mathbf{D}_{\mathrm{L,G}}^{[p,q]}}\left(\mathbf{d}_{\mathrm{L,G}}^{[p,q]}\right)$, where $\mathbf{D}_{\mathrm{L,G}}^{[p,q]}$ is defined as $\mathbf{D}_{\mathrm{L,G}}^{[p,q]} = \left\{\mathbf{A}_a^{[p,q]}, \mathbf{V}_{\mathrm{F,LCO}}^{[p,q]}\right\}$, and the n_{G}-dimensional (with $n_{\mathrm{G}} = 1 + n_{\mathrm{LCO}}$) vector $\mathbf{V}_{\mathrm{F,LCO}}^{[p,q]}$ is given by $\mathbf{V}_{\mathrm{F,LCO}}^{[p,q]} = \left\{V_{\mathrm{F}}^{[p,q]}, \mathbf{V}_{\mathrm{LCO}}^{[p,q]}\right\}$. The flutter velocity represents the lowest velocity at which flutter occurs, whereas each of the n_{LCO} LCO velocities, collected in the random vector $\mathbf{V}_{\mathrm{LCO}}^{[p,q]}$, indicates the velocity at which the corresponding LCO amplitude (e.g., maximum wing tip displacement or twist amplitude) reaches a predefined limit threshold.

Once the joint PDF $f_{\mathbf{D}_{\mathrm{L,G}}^{[p,q]}}\left(\mathbf{d}_{\mathrm{L,G}}^{[p,q]}\right) = f_{\mathbf{A}_a^{[p,q]}, \mathbf{V}_{\mathrm{F,LCO}}^{[p,q]}}\left(\mathbf{a}_a^{[p,q]}, \mathbf{v}_{\mathrm{F,LCO}}^{[p,q]}\right)$ is determined, the probability of *system failure* at time t_p^q, $P\left[F_{\mathrm{sys}}^{[p,q]}\right]$, is estimated by performing component and system reliability analyses [17]. These analyses are part of the fifth step of the framework, namely *damage prognosis analysis*, through three substeps: (i) computation of the modal conditional failure probabilities, $P\left[F_{\mathrm{L},ij}^{[p,q]} \middle| \mathbf{a}_a^{[p,q]}\right]$ and $P\left[F_{\mathrm{G},r}^{[p,q]} \middle| \mathbf{v}_{\mathrm{F,LCO}}^{[p,q]}\right]$, (ii) computation of the unconditional modal failure probabilities, $P\left[F_{\mathrm{L},ij}^{[p,q]}\right]$ and $P\left[F_{\mathrm{G},r}^{[p,q]}\right]$, and (iii) computation of the lower and upper bounds for $P\left[F_{\mathrm{sys}}^{[p,q]}\right]$.

Using the assumptions stated in the current section, and the notation $dP[X] = P[x < X \le x + dx] = f_X(x)dx$, the probability of *system failure* at time t_p^q can be obtained by using the total probability theorem (TPT) multiple times in a nested fashion as

$$
\begin{aligned}
P\left[F_{\mathrm{sys}}^{[p,q]}\right] &= \int_{\mathbf{D}_{\mathrm{L,G}}^{[p,q]}} P\left[F_{\mathrm{sys}}^{[p,q]} \middle| \mathbf{D}_{\mathrm{L,G}}^{[p,q]}\right] dP\left[\mathbf{D}_{\mathrm{L,G}}^{[p,q]}\right] \\
&= \int_{\mathbf{A}_a^{[p,q]}} \int_{\mathbf{V}_{\mathrm{F,LCO}}^{[p,q]}} P\left[F_{\mathrm{sys}}^{[p,q]} \middle| \mathbf{A}_a^{[p,q]}, \mathbf{V}_{\mathrm{F,LCO}}^{[p,q]}\right] dP\left[\mathbf{A}_a^{[p,q]}, \mathbf{V}_{\mathrm{F,LCO}}^{[p,q]}\right], \qquad (1)
\end{aligned}
$$

where the term $dP\left[\mathbf{D}_{\mathrm{L,G}}^{[p,q]}\right] = dP\left[\mathbf{A}_a^{[p,q]}, \mathbf{V}_{\mathrm{F,LCO}}^{[p,q]}\right]$ can be expressed as

$$
\begin{aligned}
dP&\left[\mathbf{A}_a^{[p,q]}, \mathbf{V}_{\mathrm{F,LCO}}^{[p,q]}\right] \\
&= \int_{\boldsymbol{\Theta}_{\mathrm{mat}}} \int_{\boldsymbol{\Theta}_{\mathrm{dam}}} dP\left[\mathbf{V}_{\mathrm{F,LCO}}^{[p,q]} \middle| \mathbf{A}_a^{[p,q]}, \boldsymbol{\Theta}_{\mathrm{mat}}, \boldsymbol{\Theta}_{\mathrm{dam}}\right] \\
&\quad \times dP\left[\mathbf{A}_a^{[p,q]} \middle| \boldsymbol{\Theta}_{\mathrm{mat}}, \boldsymbol{\Theta}_{\mathrm{dam}}\right] dP\left[\boldsymbol{\Theta}_{\mathrm{mat}}\right] dP\left[\boldsymbol{\Theta}_{\mathrm{dam}}\right], \qquad (2)
\end{aligned}
$$

and the quantity $dP\left[\mathbf{A}_a^{[p,q]} \middle| \boldsymbol{\Theta}_{\mathrm{mat}}, \boldsymbol{\Theta}_{\mathrm{dam}}\right]$ can be obtained as [15]

$$
\begin{aligned}
dP&\left[\mathbf{A}_a^{[p,q]} \middle| \boldsymbol{\Theta}_{\mathrm{mat}}, \boldsymbol{\Theta}_{\mathrm{dam}}\right] \\
&= \int_{\mathbf{A}_a^p} \int_{\mathbf{IM}} \int_{\boldsymbol{\Theta}_{\mathrm{F}}} dP\left[\mathbf{A}_a^{[p,q]} \middle| \boldsymbol{\Theta}_{\mathrm{mat}}, \boldsymbol{\Theta}_{\mathrm{dam}}, \mathbf{A}_a^p, \mathbf{IM}, \boldsymbol{\Theta}_{\mathrm{F}}\right] \\
&\quad \times dP''\left[\mathbf{A}_a^p \middle| \boldsymbol{\Theta}_{\mathrm{mat}}, \boldsymbol{\Theta}_{\mathrm{dam}}\right] \cdot dP\left[\mathbf{IM} \middle| \boldsymbol{\Theta}_{\mathrm{F}}\right] \cdot dP\left[\boldsymbol{\Theta}_{\mathrm{F}}\right]. \qquad (3)
\end{aligned}
$$

Finally, the term $dP\left[\mathbf{IM} \middle| \boldsymbol{\Theta}_{\mathrm{F}}\right]$ can conceptually be written as the product of two s.i. subterms as

$$
\begin{aligned}
dP\left[\mathbf{IM} | \boldsymbol{\Theta}_{\mathrm{F}}\right] &= dP\left[\mathbf{IM}_{\mathrm{T}}, \mathbf{IM}_{\mathrm{M}} | \boldsymbol{\Theta}_{\mathrm{F}}\right] \\
&= \int_{\boldsymbol{\Theta}_{\mathrm{T}}} dP\left[\mathbf{IM}_{\mathrm{T}} | \boldsymbol{\Theta}_{\mathrm{T}}, \boldsymbol{\Theta}_{\mathrm{F}}\right] \cdot dP\left[\boldsymbol{\Theta}_{\mathrm{T}} | \boldsymbol{\Theta}_{\mathrm{F}}\right] \\
&\quad \times \int_{\boldsymbol{\Theta}_{\mathrm{M}}} dP\left[\mathbf{IM}_{\mathrm{M}} | \boldsymbol{\Theta}_{\mathrm{M}}, \boldsymbol{\Theta}_{\mathrm{F}}\right] \cdot dP\left[\boldsymbol{\Theta}_{\mathrm{M}} | \boldsymbol{\Theta}_{\mathrm{F}}\right]. \qquad (4)
\end{aligned}
$$

The ultimate step allowed by the proposed methodology consists of the *decision-making* process. It essentially uses the damage prognosis results to optimize the maintenance and repair programs, and consequently reduce the life-cycle cost of the structure. The decisions made at current time t_p can be revised later (at times t_{p+1}, t_{p+2}, etc.) as new NDE data are collected, a concept illustrated in Fig. 3. Scheduling of the next maintenance or repair is obtained by estimating the time at which $P\left[F_{\mathrm{sys}}^{[p,q]}\right]$ will exceed a specified safety threshold $\bar{p}_{\mathrm{F}}$ [15].

3. Recursive Bayesian inference analysis

The following three assumptions regarding an NDE inspection are made herein. (i) An NDE inspection can detect and locate damage, identify the damage mechanisms simultaneously evolving at a certain damage location, and, in the best-case scenario, quantify the damage extents – by using, for instance, an equivalent damage size – for each damage mechanism detected and identified. (ii) The overall uncertainty (i.e., including both systematic and random errors) in the measured extent of damage is dependent on damage location [15], damage mechanism, and extent of damage [18]. (iii) Detection and measurement of the extent of a certain damage mechanism evolving at a certain damage location only depend on the true (and unknown) damage size of that particular damage mechanism at the time of inspection.

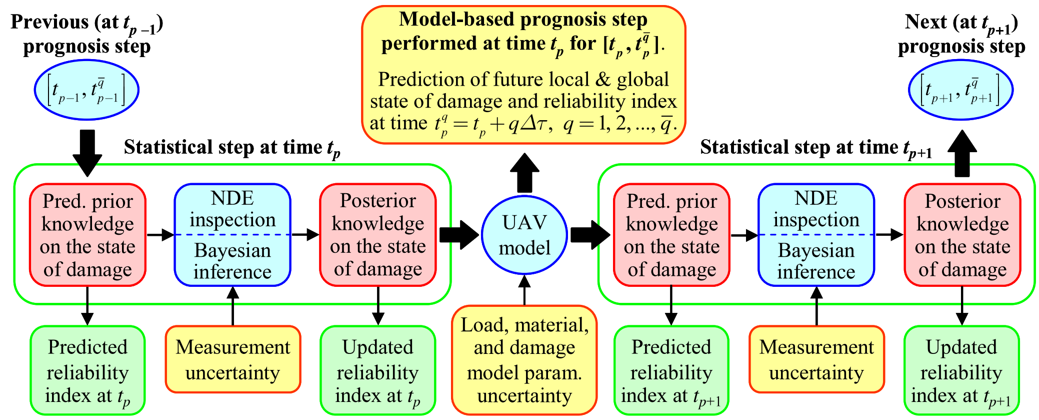

Fig. 3. Conceptual representation of proposed damage prognosis algorithm for two successive NDE inspections (at times t_p and t_{p+1}), emphasizing the alternative and recursive use of statistical and predictive analysis steps.

The detection capability of a particular NDE technique is quantified by the so-called *probability of detection* (*POD*). The *POD*, for a particular (i, j, p) combination, is defined as the probability of detecting damage of any size (i.e., $A_m^{(i,j,p)} > 0$), given that the actual damage size, at current time t_p, is $A_a^{(i,j,p)} = a_a^{(i,j,p)}$ (with $a_a^{(i,j,p)} > 0$), i.e.,

$$POD\left(a_a^{(i,j,p)}\right) = P\left[A_m^{(i,j,p)} > 0 \mid A_a^{(i,j,p)} = a_a^{(i,j,p)}\right]. \tag{5}$$

On the other hand, the probability that the NDE outcome constitutes a false alarm – i.e., damage detected ($A_m^{(i,j,p)} > 0$) when in reality there is no actual damage ($a_a^{(i,j,p)} = 0$) – is referred to as *false-call probability (FCP)* and is defined as

$$FCP_{(i,j,p)} = P\left[A_m^{(i,j,p)} > 0 \mid A_a^{(i,j,p)} = 0\right] = POD\left(a_a^{(i,j,p)} = 0\right). \tag{6}$$

The two pieces of information provided in Eqs. (5) and (6), with the former viewed as a continuous function of $a_a^{(i,j,p)}$, are combined together in the so-called *POD curve*. Several parametric models, for defining a *POD* curve from the curve fit of experimental binary data (i.e., $A_m^{(i,j,p)} > 0 \mid A_a^{(i,j,p)} = a_a^{(i,j,p)}$ and $A_m^{(i,j,p)} = 0 \mid A_a^{(i,j,p)} = a_a^{(i,j,p)}$), can be found in the literature. Among these models, those proposed by Berens [19] and Staat [20] are shown below:

$$POD\left(a_a^{(i,j,p)}\right) = \frac{\exp\left\{-\alpha_0^{(i,j)} + \alpha_1^{(i,j)} \ln\left[a_a^{(i,j,p)}\right]\right\}}{1 + \exp\left\{-\alpha_0^{(i,j)} + \alpha_1^{(i,j)} \ln\left[a_a^{(i,j,p)}\right]\right\}} \tag{7}$$

$$POD\left(a_a^{(i,j,p)}\right) = \left(1 - p_\infty^{(i,j)}\right)\left[1 - \exp\left(-\alpha_2^{(i,j)} a_a^{(i,j,p)}\right)\right]. \tag{8}$$

The terms $\alpha_0^{(i,j)}$, $\alpha_1^{(i,j)}$, and $\alpha_2^{(i,j)}$ are regression coefficients, and $p_\infty^{(i,j)}$ accounts for the fact that the *POD* for a very large damage size, $a_a^{(i,j,p)}$, is not necessarily equal to 1. The *POD* curves that can be obtained from Eqs. (7) and (8), for some particular values of the regression coefficients mentioned above, are depicted in Fig. 4.

For a particular (i, j, p) combination, once damage is detected and its extent measured, it is natural to question the fidelity/precision of that NDE measurement conditional on the actual damage size. To this end, the NDE measurement accuracy is herein accounted for by the following (linear) damage-size measurement model, used by Zhang and Mahadevan [21]:

$$A_m^{(i,j,p)}\left(A_a^{(i,j,p)} = a_a^{(i,j,p)}\right) = \beta_0^{(i,j)} + \beta_1^{(i,j)} a_a^{(i,j,p)} + \varepsilon_{ij}, \tag{9}$$

where the random variables $A_a^{(i,j,p)}$ and $A_m^{(i,j,p)}$ are respectively the actual and the measured damage size for damage location i, damage mechanism j, and inspection time t_p. The quantity $a_a^{(i,j,p)}$ denotes the value of the actual damage size for the particular (i, j, p) combination considered. The two terms $\beta_0^{(i,j)}$ and $\beta_1^{(i,j)}$ are the

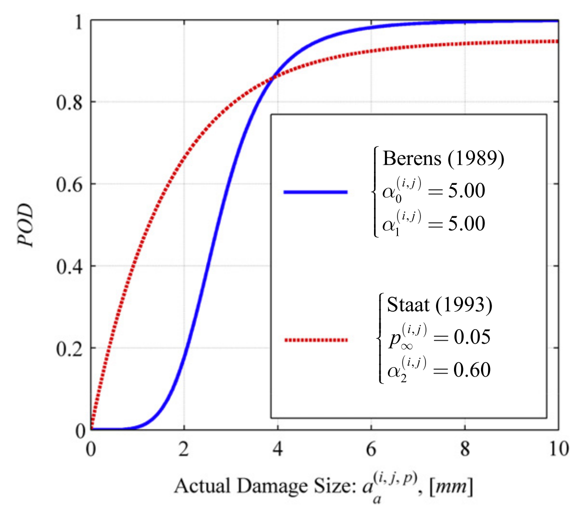

Fig. 4. Examples of two *POD* curve models found in the literature [19,20]. (For a colour version of this figure, the reader is referred to the web version of this article.)

coefficients of the (assumed) linear model in Eq. (9). Finally, $\varepsilon_{ij} \sim N\left(0, \sigma_{\varepsilon_{ij}}\right)$ represents the random measurement error/noise, assumed to be Gaussian distributed with zero-mean and standard deviation $\sigma_{\varepsilon_{ij}}$ (considered herein, for the sake of simplicity, to be independent of the actual damage size $A_a^{(i,j,p)}$ [21]). The quantities $\beta_0^{(i,j)}$, $\beta_1^{(i,j)}$, and $\sigma_{\varepsilon_{ij}}$ are unknown, and have to be estimated through a linear regression analysis [15]. The estimated linear regression coefficients and standard deviation of the random measurement error are respectively denoted $\hat{\beta}_0^{(i,j)}$, $\hat{\beta}_1^{(i,j)}$, and $\hat{\sigma}_{\varepsilon_{ij}}$. It is now possible to estimate the PDF of the measured damage size $A_m^{(i,j,p)}$, conditional on the actual damage size $A_a^{(i,j,p)} = a_a^{(i,j,p)}$ and the estimated linear regression parameters, as $f_{A_m|A_a}^{(i,j,p)}(a_m|a_a) = \varphi\left(a_m^{(i,j,p)}; \hat{\mu}_{A_m|A_a}^{(i,j,p)}, \hat{\sigma}_{\varepsilon_{ij}}\right)$, where $\varphi\left(a_m^{(i,j,p)}; \hat{\mu}_{A_m|A_a}^{(i,j,p)}, \hat{\sigma}_{\varepsilon_{ij}}\right)$ is the conditional normal PDF of $A_m^{(i,j,p)}$ with mean $\hat{\mu}_{A_m|A_a}^{(i,j,p)} = \hat{\mu}_{A_m^{(i,j,p)}|A_a^{(i,j,p)}=a_a^{(i,j,p)}} = \hat{\beta}_0^{(i,j)} + \hat{\beta}_1^{(i,j)} a_a^{(i,j,p)}$ and standard deviation $\sigma_{A_m|A_a}^{(i,j,p)} = \hat{\sigma}_{\varepsilon_{ij}}$. However, this conditional PDF is meaningful only in the range $A_m^{(i,j,p)} > 0$, and is therefore renormalized as

$$\tilde{\varphi}\left(a_m^{(i,j,p)}; \hat{\mu}_{A_m|A_a}^{(i,j,p)}, \hat{\sigma}_{\varepsilon_{ij}}\right) = \varphi\left(a_m^{(i,j,p)}; \hat{\mu}_{A_m|A_a}^{(i,j,p)}, \hat{\sigma}_{\varepsilon_{ij}}\right) \times \left[\Phi\left(\frac{\hat{\beta}_0^{(i,j)} + \hat{\beta}_1^{(i,j)} a_a^{(i,j,p)}}{\hat{\sigma}_{\varepsilon_{ij}}}\right)\right]^{-1}, \tag{10}$$

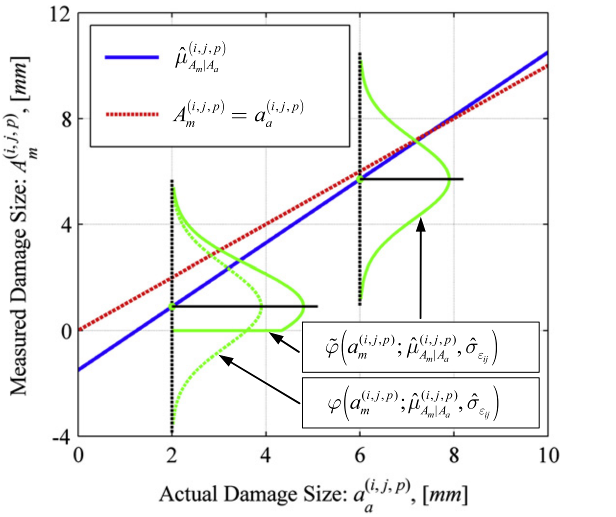

Fig. 5. Damage-size measurement model adopted in this study [21]. (For a colour version of this figure, the reader is referred to the web version of this article.)

where $\Phi(\cdot)$ represents the standard normal cumulative distribution function (CDF). All these concepts described above are illustrated in Fig. 5.

The *POD* curve and the damage size measurement model are then used to build the likelihood function, $L\left(\mathbf{a}_a^p|\mathbf{a}_m^p\right)$, needed to recursively update [10,21–23] the prior joint conditional PDF, $f'_{\mathbf{A}_a^p|\Theta_{\text{mat}},\Theta_{\text{dam}}}\left(\mathbf{a}_a^p|\boldsymbol{\theta}_{\text{mat}},\boldsymbol{\theta}_{\text{dam}}\right)$, into the posterior joint conditional PDF, $f''_{\mathbf{A}_a^p|\Theta_{\text{mat}},\Theta_{\text{dam}}}\left(\mathbf{a}_a^p|\boldsymbol{\theta}_{\text{mat}},\boldsymbol{\theta}_{\text{dam}}\right)$, as the new measurement result, $\mathbf{a}_m^p$, becomes available. This updating scheme can be written as

$$f''_{\mathbf{A}_a^p|\Theta_{\text{mat}},\Theta_{\text{dam}}}\left(\mathbf{a}_a^p|\boldsymbol{\theta}_{\text{mat}},\boldsymbol{\theta}_{\text{dam}}\right) \propto L\left(\mathbf{a}_a^p|\mathbf{a}_m^p\right) f'_{\mathbf{A}_a^p|\Theta_{\text{mat}},\Theta_{\text{dam}}}\left(\mathbf{a}_a^p|\boldsymbol{\theta}_{\text{mat}},\boldsymbol{\theta}_{\text{dam}}\right). \tag{11}$$

Furthermore, by assuming that the conditional NDE measurements $\left\{a_{m_k}^{(i,j,p)}|a_a^{(i,j,p)}, k=1,\ldots,n_{\text{MS}}^{(i,j,p)}\right\}$ (where $n_{\text{MS}}^{(i,j,p)}$ is the number of NDE measurements performed at time t_p, at location i, for damage mechanism j) are realizations from s.i. random variables for every (i,j) combination, Eq. (11) can be rewritten as

$$f''_{\mathbf{A}_a^p|\Theta_{\text{mat}},\Theta_{\text{dam}}}\left(\mathbf{a}_a^p|\boldsymbol{\theta}_{\text{mat}},\boldsymbol{\theta}_{\text{dam}}\right) \propto \left[\prod_{i=1}^{n_{\text{L}}^p}\prod_{j=1}^{n_{\text{DM}}^{(i,p)}}\prod_{k=1}^{n_{\text{MS}}^{(i,j,p)}} L\left(a_a^{(i,j,p)}\middle|a_{m_k}^{(i,j,p)}\right)\right] \times f'_{\mathbf{A}_a^p|\Theta_{\text{mat}},\Theta_{\text{dam}}}\left(\mathbf{a}_a^p|\boldsymbol{\theta}_{\text{mat}},\boldsymbol{\theta}_{\text{dam}}\right), \tag{12}$$

where n_{L}^p denotes the number of inspected damage locations at time t_p and $n_{\text{DM}}^{(i,p)}$ represents the number of detected damage mechanisms at location i at time t_p. The vector $\mathbf{A}_a^p = \{\mathbf{A}_a^{(i,p)}, i = 1,\ldots,n_{\text{L}}^{[0,p]}\}$, with $\mathbf{A}_a^{(i,p)} = \{\mathbf{A}_a^{(i,j,p)}, j=1,\ldots,n_{\text{DM}}^{(i,[0,p])}\}$, represents the collection of the actual damage sizes at all inspected locations and all detected damage mechanisms up to time t_p. Additionally, $n_{\text{L}}^{[0,p]}$ represents the total number of damage locations inspected up to time t_p, and $n_{\text{DM}}^{(i,[0,p])}$ denotes the total number of detected damage mechanisms at location i up to time t_p. The size (at time t_p) of the damage size vector $\mathbf{A}_a^p$ is thus equal to $n_{\text{A}}^p = \sum_{i=1}^{n_{\text{L}}^{[0,p]}} n_{\text{DM}}^{(i,[0,p])}$. On the other hand, the vector $\mathbf{a}_m^p = \{\mathbf{a}_m^{(i,p)}, i=1,\ldots,n_{\text{L}}^p\}$ – with its subvectors defined as $\mathbf{a}_m^{(i,p)} = \{\mathbf{a}_m^{(i,j,p)}, j=1,\ldots,n_{\text{DM}}^{(i,p)}\}$ and $\mathbf{a}_m^{(i,j,p)} = \{\mathbf{a}_{m_k}^{(i,j,p)}, k=1,\ldots,n_{\text{MS}}^{(i,j,p)}\}$ – collects all the $n_{\text{MS}}^p = \sum_{i=1}^{n_{\text{L}}^p}\sum_{j=1}^{n_{\text{DM}}^{(i,p)}} n_{\text{MS}}^{(i,j,p)}$ NDE measurement results obtained at time t_p. Finally, $L\left(a_a^{(i,j,p)}|a_{m_k}^{(i,j,p)}\right)$ represents the likelihood function of $a_a^{(i,j,p)}$ given the kth NDE measurement result, $a_{m_k}^{(i,j,p)}$. It should be noted that (i) the equality $L\left(\mathbf{a}_a^p|a_{m_k}^{(i,j,p)}\right) = L\left(a_a^{(i,j,p)}|a_{m_k}^{(i,j,p)}\right)$ is a direct consequence of the measurement model used in Eq. (9), and (ii) the mathematical form of the likelihood function depends on the NDE inspection outcome, $a_{m_k}^{(i,j,p)}$, as

$$L\left(a_a^{(i,j,p)}|a_{m_k}^{(i,j,p)}\right) = \begin{cases} \tilde{\varphi}\left(a_{m_k}^{(i,j,p)}; \hat{\mu}^{(i,j,p)}_{A_m|A_a}, \hat{\sigma}_{\varepsilon_{ij}}\right)\cdot POD\left(a_a^{(i,j,p)}\right) & \text{if } a_{m_k}^{(i,j,p)} > 0 \\ 1 - POD\left(a_a^{(i,j,p)}\right) & \text{if } a_{m_k}^{(i,j,p)} = 0. \end{cases} \tag{13}$$

It must also be mentioned that (i) the initial (i.e., at time t_0) damage-size PDF model, $f'_{\mathbf{A}_a^0}\left(\mathbf{a}_a^0\right)$, is defined on the basis of engineering judgment [10], and (ii) the components of the random vector $\mathbf{A}_a^0$, at time t_0, can be reasonably considered mutually s.i. and s.i. of Θ_{mat} and Θ_{dam} [15].

4. Probabilistic load hazard analysis

In this study, two types of external action are considered to contribute significantly to the fatigue damage accumulation in the skin-to-spar adhesive joints of a composite wing structure: turbulence-induced and maneuver-induced loads. Turbulence is modeled as a zero-mean, isotropic, stationary (in time), and homogeneous (in space) stochastic Gaussian random velocity field, as discussed in detail by Hoblit [24] and Van Staveren [25]. Its intensity, associated with the kth flight segment in the time window $\left[t_p, t_p^{\bar{q}}\right]$, is a scalar random variable taken as the root mean square ($\Sigma_{\text{T}}^{(k)}$) of the wind velocity fluctuations. This random quantity is characterized by the conditional PDF

$$f_{\Sigma_{\text{T}}^{(k)}|\Theta_{\text{T}}^{(k)},\Theta_{\text{F}}^{(k)}}\left(\sigma_{\text{T}}^{(k)}|\boldsymbol{\theta}_{\text{T}}^{(k)},\boldsymbol{\theta}_{\text{F}}^{(k)}\right) = P_0\left(h^{(k)}\right)\delta\left(\sigma_{\text{T}}^{(K)}\right) + \frac{P_1\left(h^{(k)}\right)}{b_1\left(h^{(k)}\right)}\sqrt{\frac{2}{\pi}}\exp\left[-\frac{1}{2}\left(\frac{\sigma_{\text{T}}^{(k)}}{b_1\left(h^{(k)}\right)}\right)^2\right] + \frac{P_2\left(h^{(k)}\right)}{b_2\left(h^{(k)}\right)}\sqrt{\frac{2}{\pi}}\exp\left[-\frac{1}{2}\left(\frac{\sigma_{\text{T}}^{(k)}}{b_2\left(h^{(k)}\right)}\right)^2\right], \tag{14}$$

where $P_0(h^{(k)}), P_1(h^{(k)}), P_2(h^{(k)}), b_1(h^{(k)}), b_2(h^{(k)})$ are altitude-dependent distribution parameters collected (for each flight segment) in the vector $\Theta_{\text{T}}^{(k)}$. Another essential piece of information is provided by the spatial extent, $\Delta S_{\text{T}}^{(k)}$, of the turbulent patches during the kth flight segment. In this study, the quantity $\Delta S_{\text{T}}^{(k)}$ is considered as a random variable following an exponential distribution with mean value (collected in $\Theta_{\text{T}}^{(k)}$ and potentially dependent on $h^{(k)}$) denoted as $\mu_{\Delta S_{\text{T}}^{(k)}}$; this is an assumption that is well validated by some recorded flight data found in the literature [26,27], as shown in Fig. 6. Turbulence intensity ($\Sigma_{\text{T}}^{(k)}$) and the extent of the turbulent patches ($\Delta S_{\text{T}}^{(k)}$) are collected in the turbulence intensity measure vector $\mathbf{IM}_{\text{T}}^{(k)} = \left\{\Sigma_{\text{T}}^{(k)}, \Delta S_{\text{T}}^{(k)}\right\}$. The random sequence of the intensities of the turbulent patches during each of the n_s flight segments in $\left[t_p, t_p^{\bar{q}}\right]$ can be modeled and simulated using homogeneous Poisson rectangular pulse processes [15,31] with mean rate of occurrence $\lambda_{\text{T}}^{(k)} = 1/\mu_{\Delta S_{\text{T}}^{(k)}}$. Each arrival (in space) of a Poisson event raises a rectangular

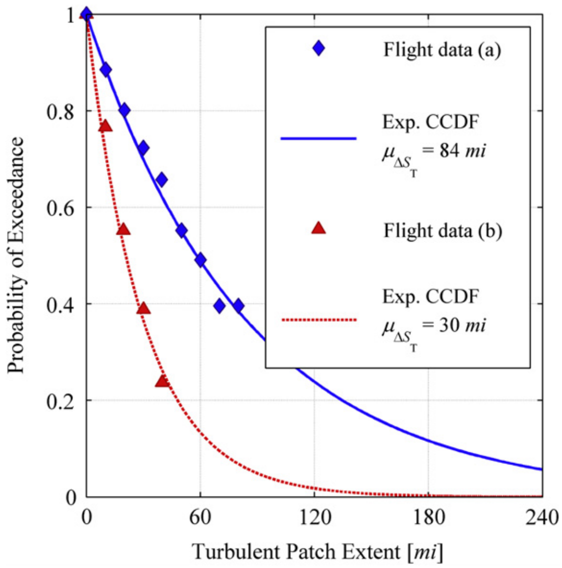

Fig. 6. Probability of turbulent patches exceeding a specified extent in different geographical areas (from Ref. [27]). (a) From flight data collected in Southern USA and altitudes above 40,000 ft. (b) From flight data collected in Western Europe and altitudes between 20,000 and 40,000 ft. The lines represent the fitted exponential complementary CDF (CCDF). (For a colour version of this figure, the reader is referred to the web version of this article.)

pulse of random intensity $\Sigma_{\mathrm{T}}^{(k)}$ – according to the conditional PDF $f_{\Sigma_{\mathrm{T}}^{(k)}|\boldsymbol{\Theta}_{\mathrm{T}}^{(k)},\boldsymbol{\Theta}_{\mathrm{F}}^{(k)}}\left(\sigma_{\mathrm{T}}^{(k)}|\boldsymbol{\theta}_{\mathrm{T}}^{(k)},\boldsymbol{\theta}_{\mathrm{F}}^{(k)}\right)$ in Eq. (14) – until the next arrival. An illustrative example is shown in Fig. 7. Additionally, a generic realization of the random vector $\mathbf{IM}_{\mathrm{T}}$ in $\left[t_p, t_p^{\bar{q}}\right]$ is herein denoted as $\mathbf{im}_{\mathrm{T}} = \left\{\mathbf{im}_{\mathrm{T}}^{(k)}, k = 1, \ldots, n_s\right\}$, where the subvector $\mathbf{im}_{\mathrm{T}}^{(k)}$ is defined as $\mathbf{im}_{\mathrm{T}}^{(k)} \triangleq \left\{\mathbf{im}_{\mathrm{T}}^{(k,m)}, m = 1, \ldots, n_{\mathrm{T}}^{(k)}\right\}$, with (i) $\mathbf{im}_{\mathrm{T}}^{(k,m)} = \left\{\sigma_{\mathrm{T}}^{(k,m)}, \Delta s_{\mathrm{T}}^{(k,m)}\right\}$ denoting the intensity and extent of the mth turbulent patch and (ii) $n_{\mathrm{T}}^{(k)}$ representing the total number of turbulence patches (within the kth flight segment) randomly generated during a generic realization of $\mathbf{IM}_{\mathrm{T}}^{(k)}$. Once an ensemble of turbulence intensity time histories in $\left[t_p, t_p^{\bar{q}}\right]$ is generated, Von Karman or Dryden turbulence velocity spectra are then used (as described in Ref. [25]) to stochastically realize an ensemble of 1-, 2-, or 3-dimensional spatially correlated turbulence velocity paths for each turbulence intensity $\sigma_{\mathrm{T}}^{(k,m)}$ realized in the previous step. These paths are subsequently employed, together with the remaining flight profile information stored in $\boldsymbol{\Theta}_{\mathrm{F}}$ (e.g., $\left\{\mathbf{V}^{(k)}, k = 1, \ldots, n_s\right\}$ and $\left\{T^{(k)}, k = 1, \ldots, n_s\right\}$), to generate the ensemble of time histories of the turbulence-induced loads for each flight segment in $\left[t_p, t_p^{\bar{q}}\right]$.

On the other hand, the maneuver-induced loads experienced during the kth flight segment are characterized by (i) the mean rate of occurrence of maneuvers during that segment, $\lambda_{\mathrm{M}}^{(k)}$ (collected in $\boldsymbol{\Theta}_{\mathrm{M}}^{(k)}$, and assumed here to be a deterministic function of $\boldsymbol{\Theta}_{\mathrm{F}}^{(k)}$), (ii) the maneuver-induced load factor, $Z_{\mathrm{M}}^{(k)}$ (see Ref. [15]), and (iii) the maneuver duration, $\Delta T_{\mathrm{M}}^{(k)}$, also represented by a random variable (renewed at each occurrence of a maneuver) following an exponential distribution with mean value $\mu_{\Delta T_{\mathrm{M}}^{(k)}}$. The maneuver-induced load factor and maneuver duration are collected in the vector $\mathbf{IM}_{\mathrm{M}}^{(k)}$ as $\mathbf{IM}_{\mathrm{M}}^{(k)} = \left\{Z_{\mathrm{M}}^{(k)}, \Delta T_{\mathrm{M}}^{(k)}\right\}$. These measures are typically characterized on the basis of flight data [28–30], from which it is possible to (i) derive $\lambda_{\mathrm{M}}^{(k)}$ as a function, for instance, of the altitude of flight, (ii) assign a certain PDF, $f_{Z_{\mathrm{M}}^{(k)}}\left(\zeta_{\mathrm{M}}^{(k)}\right)$, to the load factor, $Z_{\mathrm{M}}^{(k)}$, and (iii) estimate the mean value, $\mu_{\Delta T_{\mathrm{M}}^{(k)}}$, of the maneuver duration within a given flight segment. The time histories of the maneuver-induced loads are modeled and simulated as censored homogeneous Poisson rectangular pulse processes with mean rate of occurrence $\lambda_{\mathrm{M}}^{(k)}$ for the random arrival in time of the rectangular pulses [15,31]. The random components $Z_{\mathrm{M}}^{(k)}$ and $\Delta T_{\mathrm{M}}^{(k)}$ can in general be statistically correlated and their statistical parameters – such as the mean value of the maneuver duration, $\mu_{\Delta T_{\mathrm{M}}^{(k)}}$, and the distribution parameters of the PDF $f_{Z_{\mathrm{M}}^{(k)}}\left(\zeta_{\mathrm{M}}^{(k)}\right)$ – are collected (for each flight segment) in the vector $\boldsymbol{\Theta}_{\mathrm{M}} = \left\{\boldsymbol{\Theta}_{\mathrm{M}}^{(k)}, k = 1, \ldots, n_s\right\}$. Finally, with a notation very similar to the one used previously in this section, a generic realization of the random vector $\mathbf{IM}_{\mathrm{M}}$ is denoted $\mathbf{im}_{\mathrm{M}} = \left\{\mathbf{im}_{\mathrm{M}}^{(k)}, k = 1, \ldots, n_s\right\}$, where the subvector $\mathbf{im}_{\mathrm{M}}^{(k)}$ is defined as $\mathbf{im}_{\mathrm{M}}^{(k)} \triangleq \left\{\mathbf{im}_{\mathrm{M}}^{(k,m)}, m = 1, \ldots, n_{\mathrm{M}}^{(k)}\right\}$, with (i) $\mathbf{im}_{\mathrm{M}}^{(k,m)} = \left\{\zeta_{\mathrm{M}}^{(k,m)}, \Delta t_{\mathrm{M}}^{(k)}\right\}$ denoting the intensity and duration of the mth maneuver and (ii) $n_{\mathrm{M}}^{(k)}$ representing the total number of maneuvers (within the kth flight segment) randomly generated in a generic

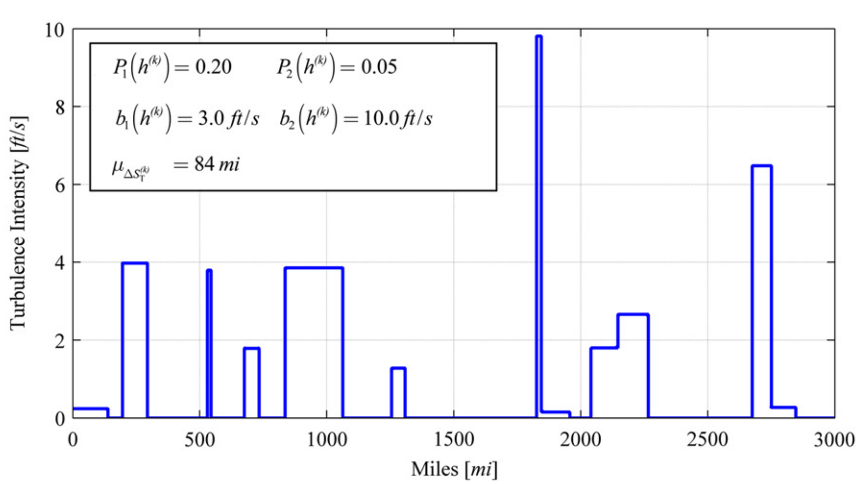

Fig. 7. Illustrative example of the homogeneous Poisson rectangular pulse process used as the stochastic model for the turbulence-induced intensities (within the kth flight segment) for a given set of turbulence distribution parameters and an average turbulence patch extent of 84 miles (i.e., the average extent from flight data collected in Southern USA from Fig. 5-b).

realization of $\mathbf{IM}_{\mathrm{M}}^{(k)}$. Further insight on the modeling and simulation of maneuver-induced loads is provided in Ref. [15].

5. Probabilistic structural response analysis

Once the two types of aerodynamic load intensity measure are characterized probabilistically, the joint conditional PDF $f_{\mathbf{A}_a^{[p,q]}|\boldsymbol{\Theta}_{\mathrm{mat}},\boldsymbol{\Theta}_{\mathrm{dam}}}\left(\mathbf{a}_a^{[p,q]}|\boldsymbol{\theta}_{\mathrm{mat}},\boldsymbol{\theta}_{\mathrm{dam}}\right)$, at time $t_p^q = t_p + q\Delta\tau$ (with $q = 1, 2, \ldots, \bar{q}$), is computed through extensive MC simulations during which the random vectors $\mathbf{A}_a^p$, $\mathbf{IM}$, and $\boldsymbol{\Theta}_{\mathrm{F}}$ are sampled according to their PDFs – i.e., $f''_{\mathbf{A}_a^p|\boldsymbol{\Theta}_{\mathrm{mat}},\boldsymbol{\Theta}_{\mathrm{dam}}}\left(\mathbf{a}_a^p|\boldsymbol{\theta}_{\mathrm{mat}},\boldsymbol{\theta}_{\mathrm{dam}}\right)$, $f_{\mathbf{IM}|\boldsymbol{\Theta}_{\mathrm{F}}}(\mathbf{im}|\boldsymbol{\theta}_{\mathrm{F}})$, and $f_{\boldsymbol{\Theta}_{\mathrm{F}}}(\boldsymbol{\theta}_{\mathrm{F}})$ – in the application of the TPT shown in Eq. (3). The uncertainty of $\mathbf{A}_a^{[p,q]}$ for given/fixed values of $\boldsymbol{\Theta}_{\mathrm{mat}} = \boldsymbol{\theta}_{\mathrm{mat}}$, $\boldsymbol{\Theta}_{\mathrm{dam}} = \boldsymbol{\theta}_{\mathrm{dam}}$, $\mathbf{A}_a^p = \mathbf{a}_a^p$, $\mathbf{IM} = \mathbf{im}$, and $\boldsymbol{\Theta}_{\mathrm{F}} = \boldsymbol{\theta}_{\mathrm{F}}$ arises from the record-to-record variability of the structural response across the ensemble of turbulence paths stochastically realized for a given value of the turbulence intensity. Therefore, providing the complete probabilistic characterization of $f_{\mathbf{A}_a^{[p,q]}|\boldsymbol{\Theta}_{\mathrm{mat}},\boldsymbol{\Theta}_{\mathrm{dam}},\mathbf{A}_a^p,\mathbf{IM},\boldsymbol{\Theta}_{\mathrm{F}}}\left(\mathbf{a}_a^{[p,q]}|\boldsymbol{\theta}_{\mathrm{mat}},\boldsymbol{\theta}_{\mathrm{dam}},\mathbf{a}_a^p,\mathbf{im},\boldsymbol{\theta}_{\mathrm{F}}\right)$ and solving Eq. (3) represents a formidable task. Under this perspective, estimating the conditional mean $\bar{\mathbf{a}}_a^{[p,q]} = \bar{\mathbf{a}}_a^{[p,q]}(\boldsymbol{\theta}_{\mathrm{mat}},\boldsymbol{\theta}_{\mathrm{dam}},\mathbf{a}_a^p,\mathbf{im},\boldsymbol{\theta}_{\mathrm{F}}) = E_{\mathrm{ens}}\left[\mathbf{A}_a^{[p,q]}|\boldsymbol{\theta}_{\mathrm{mat}},\boldsymbol{\theta}_{\mathrm{dam}},\mathbf{a}_a^p,\mathbf{im},\boldsymbol{\theta}_{\mathrm{F}}\right]$ across the ensemble of turbulence patches stochastically realized is thus a more realistic and computationally achievable goal. Following this approach, Eq. (3) can be simplified as follows [15]:

$$
\begin{aligned}
& f_{\mathbf{A}_a^{[p,q]}|\boldsymbol{\Theta}_{\mathrm{mat}},\boldsymbol{\Theta}_{\mathrm{dam}}}\left(\mathbf{a}_a^{[p,q]}|\boldsymbol{\theta}_{\mathrm{mat}},\boldsymbol{\theta}_{\mathrm{dam}}\right) \\
& \quad = \int_{\mathbf{A}_a^p}\int_{\mathbf{IM}}\int_{\boldsymbol{\Theta}_{\mathrm{F}}} \delta\left(\mathbf{a}_a^{[p,q]} - \bar{\mathbf{a}}_a^{[p,q]}\right) \\
& \qquad \times f''_{\mathbf{A}_a^p|\boldsymbol{\Theta}_{\mathrm{mat}},\boldsymbol{\Theta}_{\mathrm{dam}}}\left(\mathbf{a}_a^p|\boldsymbol{\theta}_{\mathrm{mat}},\boldsymbol{\theta}_{\mathrm{dam}}\right) f_{\mathbf{IM}|\boldsymbol{\Theta}_{\mathrm{F}}}(\mathbf{im}|\boldsymbol{\theta}_{\mathrm{F}}) \\
& \qquad \times f_{\boldsymbol{\Theta}_{\mathrm{F}}}(\boldsymbol{\theta}_{\mathrm{F}}) d\mathbf{a}_a^p \, d\mathbf{im} \, d\boldsymbol{\theta}_{\mathrm{F}}.
\end{aligned} \tag{15}
$$

The use of metamodels – such as polynomial response surface models [16] and Gaussian Process (GP) models [32] – has to be considered in order to efficiently compute $f_{\mathbf{A}_a^{[p,q]}|\boldsymbol{\Theta}_{\mathrm{mat}},\boldsymbol{\Theta}_{\mathrm{dam}}}(\mathbf{a}_a^{[p,q]}|\boldsymbol{\theta}_{\mathrm{mat}},\boldsymbol{\theta}_{\mathrm{dam}})$. This joint conditional PDF is obtained by computing the quantity $\mathbf{a}_a^{[p,q]}$, through a series of MC simulations (performed using the metamodel) during which the input parameters $\mathbf{a}_a^p$, $\mathbf{im}$, and $\boldsymbol{\theta}_{\mathrm{F}}$ are sampled from their joint PDFs, while the samples from the random parameter vectors $\boldsymbol{\theta}_{\mathrm{mat}}$ and $\boldsymbol{\theta}_{\mathrm{dam}}$ are kept constant [15]. Following a dimensional analysis approach [33,34] applied to the specific case studied herein, a possible mathematical form for the metamodel capable of providing (as output) the average rate of fatigue-induced damage propagation (across the ensemble of the turbulence paths realized) for a given set of the input parameters is given by

$$
\begin{aligned}
& E_{\mathrm{ens}}\left[\frac{d}{dt}\left(\mathbf{A}_a^{[p,t]}\,\middle|\,\boldsymbol{\theta}_{\mathrm{mat}},\boldsymbol{\theta}_{\mathrm{dam}},\mathbf{a}_a^p,\mathbf{im},\boldsymbol{\theta}_{\mathrm{F}}\right)\right] \\
& \quad = \mathbf{G}\left(\bar{\mathbf{a}}_a^{[p,t]},\mathbf{v},\zeta_{\mathrm{M}},\sigma_{\mathrm{T}};\boldsymbol{\theta}_{\mathrm{mat}},\boldsymbol{\theta}_{\mathrm{dam}}\right),
\end{aligned} \tag{16}
$$

where $E_{\mathrm{ens}}\left[d\left(\mathbf{A}_a^{[p,t]}\,\middle|\,\boldsymbol{\theta}_{\mathrm{mat}},\boldsymbol{\theta}_{\mathrm{dam}},\mathbf{a}_a^p,\mathbf{im},\boldsymbol{\theta}_{\mathrm{F}}\right)/dt\right]$ – with dt being a "macro" increment of time expressed in flight hours – represents the expected rate of damage propagation at time $t \geq t_p$ for fixed values of $\boldsymbol{\theta}_{\mathrm{mat}}$, $\boldsymbol{\theta}_{\mathrm{dam}}$, $\mathbf{a}_a^p$, $\mathbf{im}$, and $\boldsymbol{\theta}_{\mathrm{F}}$; the vector $\bar{\mathbf{a}}_a^{[p,t]}$ (of length n_{A}^p) represents the conditional expectation of the damage-size vector (at time $t \geq t_p$) defined as $\bar{\mathbf{a}}_a^{[p,t]} = \bar{\mathbf{a}}_a^{[p,t]}\left(\boldsymbol{\theta}_{\mathrm{mat}},\boldsymbol{\theta}_{\mathrm{dam}},\mathbf{a}_a^p,\mathbf{im},\boldsymbol{\theta}_{\mathrm{F}}\right) = E_{\mathrm{ens}}\left[\mathbf{A}_a^{[p,t]}\,\middle|\,\boldsymbol{\theta}_{\mathrm{mat}},\boldsymbol{\theta}_{\mathrm{dam}},\mathbf{a}_a^p,\mathbf{im},\boldsymbol{\theta}_{\mathrm{F}}\right]$; the three-component vector $\mathbf{v}$ quantifies the velocity of the mean airstream w.r.t. a reference system fixed to the aircraft; ζ_{M} defines a particular realization of the maneuver-induced load factor; and σ_{T} characterizes the intensity of the turbulence field. The general nonlinear mapping $\mathbf{G}(\cdot): \mathbb{R}^{n_{\mathrm{inp}}} \to \mathbb{R}_+^{n_{\mathrm{A}}^p}$ (with $n_{\mathrm{inp}} = n_{\mathrm{A}}^p + 5 + n_{\mathrm{mat}} + n_{\mathrm{dam}}$), between the input and output real vector spaces, represents the metamodel fitted (through an appropriate and computationally feasible *design of experiments*) over the desired design space for the input parameters using the simulation results from the (physics-based) nonlinear FE model of the composite wing. Furthermore, if the condition for mean square differentiability of the random process $\left(\mathbf{A}_a^{[p,t]}\,\middle|\,\boldsymbol{\theta}_{\mathrm{mat}},\boldsymbol{\theta}_{\mathrm{dam}}^p,\mathbf{a}_a^p,\mathbf{im}\right)$ is satisfied, the expectation and differentiation operators can permute, and Eq. (16) can be rewritten as

$$
\begin{cases}
\dfrac{d}{dt}\bar{\mathbf{a}}_a^{[p,t]} = \mathbf{G}\left(\bar{\mathbf{a}}_a^{[p,t]},\mathbf{v},\zeta_{\mathrm{M}},\sigma_{\mathrm{T}};\boldsymbol{\theta}_{\mathrm{mat}},\boldsymbol{\theta}_{\mathrm{dam}}\right) \\
\bar{\mathbf{a}}_a^p = \mathbf{a}_a^p,
\end{cases} \tag{17}
$$

where $\bar{\mathbf{a}}_a^p$ represents the value of the vector $\bar{\mathbf{a}}_a^{[p,t]}$ at time $t = t_p$ and $\mathbf{a}_a^p$ is a particular realization of $\mathbf{A}_a^p$ according to the posterior joint PDF $f''_{\mathbf{A}_a^p|\boldsymbol{\Theta}_{\mathrm{mat}},\boldsymbol{\Theta}_{\mathrm{dam}}}\left(\mathbf{a}_a^p|\boldsymbol{\theta}_{\mathrm{mat}},\boldsymbol{\theta}_{\mathrm{dam}}\right)$. Eq. (17) represents a system of first-order ordinary differential equations that can now be numerically integrated between current time t_p and t_p^q to compute $\bar{\mathbf{a}}_a^{[p,q]}$.

An exhaustive treatment of all the steps necessary to compute the conditional joint PDF $f_{\mathbf{A}_a^{[p,q]}|\boldsymbol{\Theta}_{\mathrm{mat}},\boldsymbol{\Theta}_{\mathrm{dam}}}\left(\mathbf{a}_a^{[p,q]}|\boldsymbol{\theta}_{\mathrm{mat}},\boldsymbol{\theta}_{\mathrm{dam}}\right)$ (with $q = 1, 2, \ldots, \bar{q}$) is presented in Ref. [15]. Herein, the outcome of these steps is conceptually illustrated in Fig. 8 for the case of a single damage location (i.e., $i = 1$ and $n_{\mathrm{L}}^p = n_{\mathrm{L}}^{[0,p]} = 1$) and a single damage mechanism (i.e., $j = 1$ and $n_{\mathrm{DM}}^{(1,p)} = n_{\mathrm{DM}}^{(1,[0,p])} = 1$). In this figure, a set of damage extents (sample points at time t_p), sampled according to the posterior conditional PDF $f''_{A_a^{(i,j,p)}|\boldsymbol{\Theta}_{\mathrm{mat}},\boldsymbol{\Theta}_{\mathrm{dam}}}\left(a_a^{(i,j,p)}|\boldsymbol{\theta}_{\mathrm{mat}},\boldsymbol{\theta}_{\mathrm{dam}}\right)$, is stochastically propagated at future times $t_p^q = t_p + q\Delta\tau$ with $q = 1, 2, \ldots, \bar{q}$ and $\bar{q} = 4$ (i.e., the four sets of sample points appropriately numbered in Fig. 8). Furthermore, the interpolated conditional PDF at time t_{p+1}, $f'_{A_a^{(i,j,p+1)}|\boldsymbol{\Theta}_{\mathrm{mat}},\boldsymbol{\Theta}_{\mathrm{dam}}}\left(a_a^{(i,j,p+1)}|\boldsymbol{\theta}_{\mathrm{mat}},\boldsymbol{\theta}_{\mathrm{dam}}\right)$, is also highlighted in Fig. 8 through the set of sample points between time $t_p^2 = t_p + 2\Delta\tau$ and time $t_p^3 = t_p + 3\Delta\tau$. This conditional PDF is used as prior information for the next Bayesian updating, aimed at computing the posterior conditional PDF $f''_{A_a^{(i,j,p+1)}|\boldsymbol{\Theta}_{\mathrm{mat}},\boldsymbol{\Theta}_{\mathrm{dam}}}\left(a_a^{(i,j,p+1)}|\boldsymbol{\theta}_{\mathrm{mat}},\boldsymbol{\theta}_{\mathrm{dam}}\right)$ at time t_{p+1}, as the next NDE inspection outcome becomes available.

6. Probabilistic flutter and limit cycle oscillation analyses

This fourth step of the methodology uses the damage evolution prediction from time t_p to time t_p^q (with $q = 1, 2, \ldots, \bar{q}$), for estimating (at future time t_p^q) the joint PDF of (i) the damage size vector $\mathbf{A}_a^{[p,q]}$, (ii) the flutter velocity $V_{\mathrm{F}}^{[p,q]}$, and (iii) the vector of LCO velocities $\mathbf{V}_{\mathrm{LCO}}^{[p,q]} = \left\{V_{\mathrm{LCO}}^{(r,[p,q])},\ r = 1, \ldots, n_{\mathrm{LCO}}\right\}$. Each of the n_{LCO} LCO velocities is computed via aerodynamic analyses performed in the time domain, and they can potentially be lower – in the case of a damaged wing – than the (linear) flutter velocity [35]. The total number of global aeroelastic failure modes considered in this fourth step is therefore equal to $n_{\mathrm{G}} = 1 + n_{\mathrm{LCO}}$, and also represents the dimension of the random vector $\mathbf{V}_{\mathrm{F,LCO}}^{[p,q]} = \left\{V_{\mathrm{F,LCO}}^{(r,[p,q])}, r = 1, \ldots, n_{\mathrm{G}}\right\}$ probabilistically characterized by the joint PDF $f_{\mathbf{V}_{\mathrm{F,LCO}}^{[p,q]}}\left(\mathbf{v}_{\mathrm{F,LCO}}^{[p,q]}\right)$. The final outcome of this fourth step is represented by the joint PDF,

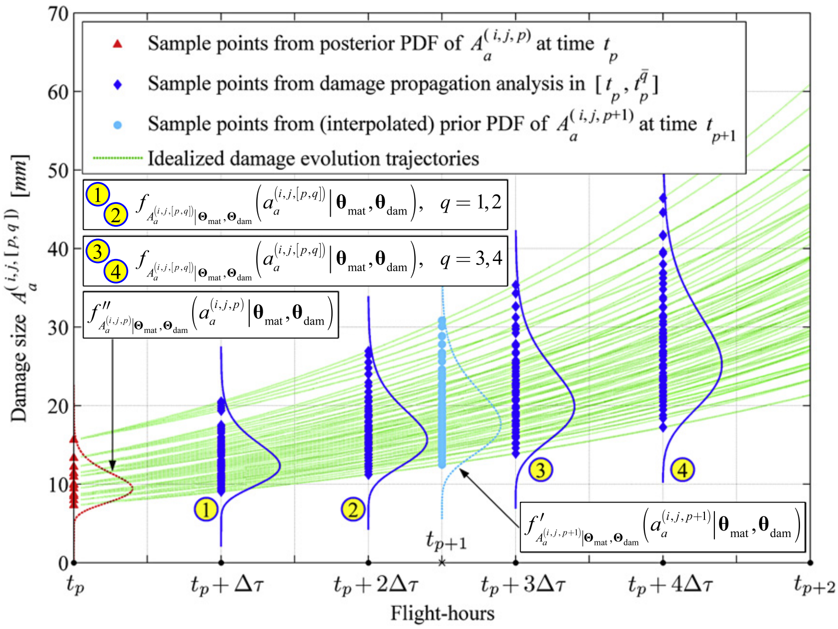

Fig. 8. Illustrative example of the proposed damage prediction approach for a particular combination of damage location (i), damage mechanism (j), and four evaluations (i.e., $\bar{q}=4$) of the damage-size PDF across the predicted (at time t_p) ensemble of damage sizes. (For a colour version of this figure, the reader is referred to the web version of this article.)

$f_{\mathbf{D}_{\mathrm{L,G}}^{[p,q]}}\left(\mathbf{d}_{\mathrm{L,G}}^{[p,q]}\right) = f_{\mathbf{A}_a^{[p,q]},\mathbf{V}_{\mathrm{F,LCO}}^{[p,q]}}\left(\mathbf{a}_a^{[p,q]}, \mathbf{v}_{\mathrm{F,LCO}}^{[p,q]}\right)$, of the random vector $\mathbf{D}_{\mathrm{L,G}}^{[p,q]} = \left\{\mathbf{A}_a^{[p,q]}, \mathbf{V}_{\mathrm{F,LCO}}^{[p,q]}\right\}$. This joint PDF can be obtained through two substeps. In the first substep, the joint conditional PDF $f_{\mathbf{V}_{\mathrm{F,LCO}}^{[p,q]}|\mathbf{A}_a^{[p,q]},\,\Theta_{\mathrm{mat}},\,\Theta_{\mathrm{dam}}}\left(\mathbf{v}_{\mathrm{F,LCO}}^{[p,q]}\,\middle|\,\mathbf{a}_a^{[p,q]},\,\boldsymbol{\theta}_{\mathrm{mat}},\,\boldsymbol{\theta}_{\mathrm{dam}}\right)$ is numerically estimated by performing multiple flutter and LCO analyses — each of them for a fixed realization of (i) the predicted (during the probabilistic damage evolution analysis) damage size vector $\mathbf{a}_a^{[p,q]}$, and (ii) the vectors $\boldsymbol{\theta}_{\mathrm{mat}}$ and $\boldsymbol{\theta}_{\mathrm{dam}}$ sampled from their PDFs $f_{\Theta_{\mathrm{mat}}}(\boldsymbol{\theta}_{\mathrm{mat}})$ and $f_{\Theta_{\mathrm{dam}}}(\boldsymbol{\theta}_{\mathrm{dam}})$ at the time of the first NDE inspection as mentioned in Section 5. In the second substep, the unconditional joint PDF of $\mathbf{D}_{\mathrm{L,G}}^{[p,q]}$ is computed according to Eq. (2).

The use of metamodels is also extremely useful in this step of the framework in order to reduce the computational cost of the probabilistic flutter and LCO analyses aimed at determining the joint conditional PDF $f_{\mathbf{V}_{\mathrm{F,LCO}}^{[p,q]}|\mathbf{A}_a^{[p,q]},\,\Theta_{\mathrm{mat}},\Theta_{\mathrm{dam}}}\left(\mathbf{v}_{\mathrm{F,LCO}}^{[p,q]}\,\middle|\,\mathbf{a}_a^{[p,q]},\,\boldsymbol{\theta}_{\mathrm{mat}},\,\boldsymbol{\theta}_{\mathrm{dam}}\right)$. It is well known that both flutter and LCO velocities are primarily governed by the stiffness, strength, and level of damage of the wing. Additionally, if the air density – which renders both the flutter and LCO velocities dependent on Θ_{F} through the altitude of flight $H^{(k)}, k = 1, \ldots, n_s$ – is considered as a deterministic quantity and assumed (as a simplification) to be independent of $H^{(k)}$, then a possible mathematical form for the metamodel is given by $\bar{\mathbf{v}}_{\mathrm{F,LCO}}^{[p,q]} = \mathbf{Q}(\mathbf{a}_a^{[p,q]};\,\boldsymbol{\theta}_{\mathrm{mat}},\,\boldsymbol{\theta}_{\mathrm{dam}})$. The vector $\bar{\mathbf{v}}_{\mathrm{F,LCO}}^{[p,q]}$, defined as $\left(\bar{\mathbf{v}}_{\mathrm{F,LCO}}^{[p,q]} = \mathbf{V}_{\mathrm{F,LCO}}^{[p,q]}\,\middle|\,\mathbf{a}_a^{[p,q]},\,\boldsymbol{\theta}_{\mathrm{mat}},\,\boldsymbol{\theta}_{\mathrm{dam}}\right)$, represents the output of the metamodel for a given set of the input parameters $\mathbf{a}_a^{[p,q]}$, $\boldsymbol{\theta}_{\mathrm{mat}}$, and $\boldsymbol{\theta}_{\mathrm{dam}}$. The function $\mathbf{Q}(\cdot):\mathbb{R}^{n_{\mathrm{inp}}} \rightarrow \mathbb{R}_+^{n_{\mathrm{G}}}$ (with $n_{\mathrm{inp}} = n_{\mathrm{A}} + n_{\mathrm{mat}} + n_{\mathrm{dam}}$) is instead a general nonlinear mapping, between the input and (positive) output real vector spaces, representing the metamodel fitted – over the desired design space for the input parameters – using the simulations from the coupled FE and aerodynamic models of the composite wing structure. Furthermore, as a direct consequence of these considerations, the joint conditional PDF of $\mathbf{V}_{\mathrm{F,LCO}}^{[p,q]}$ can be rewritten as $f_{\mathbf{V}_{\mathrm{F,LCO}}^{[p,q]}|\mathbf{A}_a^{[p,q]},\Theta_{\mathrm{mat}},\Theta_{\mathrm{dam}}}\left(\mathbf{V}_{\mathrm{F,LCO}}^{[p,q]}|\mathbf{a}_a^{[p,q]},\,\boldsymbol{\theta}_{\mathrm{mat}},\,\boldsymbol{\theta}_{\mathrm{dam}}\right) = \delta\left(\mathbf{v}_{\mathrm{F,LCO}}^{[p,q]} - \bar{\mathbf{v}}_{\mathrm{F,LCO}}^{[p,q]}\right)$, and the marginal joint PDF of the vector $\mathbf{V}_{\mathrm{F,LCO}}^{[p,q]}$ can thus be computed as

$$f_{\mathbf{V}_{\mathrm{F,LCO}}^{p,q}}\left(\mathbf{v}_{\mathrm{F,LCO}}^{[p,q]}\right) = \int_{\mathbf{A}_a^{[p,q]}}\int_{\Theta_{\mathrm{mat}}}\int_{\Theta_{\mathrm{dam}}} \delta\left(\mathbf{v}_{\mathrm{F,LCO}}^{[p,q]} - \bar{\mathbf{v}}_{\mathrm{F,LCO}}^{[p,q]}\right) \times f''_{\mathbf{A}_a^{[p,q]}|\Theta_{\mathrm{mat}},\Theta_{\mathrm{dam}}}\left(\mathbf{a}_a^{[p,q]}\,|\boldsymbol{\theta}_{\mathrm{mat}},\,\boldsymbol{\theta}_{\mathrm{dam}}\right) \times f_{\Theta_{\mathrm{mat}}}(\boldsymbol{\theta}_{\mathrm{mat}})\,f_{\Theta_{\mathrm{dam}}}(\boldsymbol{\theta}_{\mathrm{dam}}) \times d\mathbf{a}_a^{[p,q]}\,d\boldsymbol{\theta}_{\mathrm{mat}}\,d\boldsymbol{\theta}_{\mathrm{dam}}. \tag{18}$$

7. Damage prognosis analysis

The fifth step of the proposed framework – namely *damage prognosis analysis* – can be carried out in three substeps by (i) using the joint probabilistic information of the local and global states of damage at time t_p^q, and (ii) defining appropriate limit-state functions for both local and global (aeroelastic) potential failure modes. The first substep consists of computing the modal failure probability conditional on the actual damage size (for local failure modes) and the flutter or LCO velocities (for global failure modes); i.e., $P\left[F_{\mathrm{L},ij}^{[p,q]}\,\middle|\,\mathbf{a}_a^{[p,q]}\right]$ (with $i = 1, \ldots, n_{\mathrm{L}}^{[0,p]}$ and $j = 1, \ldots, n_{\mathrm{DM}}^{(i,[0,p])}$) and $P\left[F_{\mathrm{G},r}^{[p,q]}\,\middle|\,\mathbf{v}_{\mathrm{F,LCO}}^{[p,q]}\right]$ (with $r = 1, \ldots, n_{\mathrm{G}}$), respectively. In the second substep, the local and global conditional modal failure probabilities are unconditioned w.r.t. $\mathbf{A}_a^{[p,q]}$ and $\mathbf{V}_{\mathrm{F,LCO}}^{[p,q]}$, respectively, and the two outcomes are denoted by $P\left[F_{\mathrm{L},ij}^{[p,q]}\right]$ (with $i = 1, \ldots, n_{\mathrm{L}}^{[0,p]}$ and $j = 1, \ldots, n_{\mathrm{DM}}^{(i,[0,p])}$) and $P\left[F_{\mathrm{G},r}^{[p,q]}\right]$ (with $r = 1, \ldots, n_{\mathrm{G}}$). Finally, in the third and last substep, lower and upper bounds for the probability of *system failure*, $P\left[F_{\mathrm{sys}}^{[p,q]}\right]$, are computed by abstracting the composite wing structure – or any other structural component of interest – to a series system.

The local failure event $F_{\mathrm{L},ij}^{[p,q]}$ – i.e., the failure event (at time t_p^q) associated with the jth detected damage mechanism, evolving at the ith monitored damage location – can be defined as $F_{\mathrm{L},ij}^{[p,q]} \triangleq \left\{A_a^{(i,j,[p,q])} \geq a_c^{ij}\right\}$, where a_c^{ij} represents a predefined critical damage

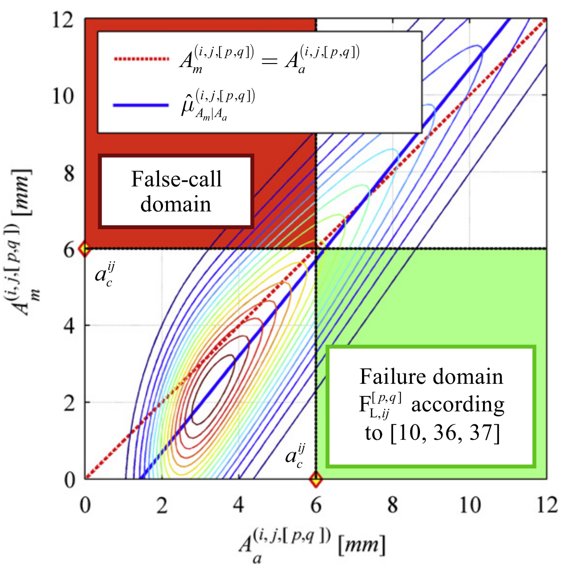

Fig. 9. Failure and false-call domains according to the local failure and false-call criteria in Eqs. (23) and (25), respectively.

size [15]. According to this definition, the conditional modal failure probability $P\left[F_{L,ij}^{[p,q]}\middle|\mathbf{a}_a^{[p,q]}\right]$ is given by

$$P\left[F_{L,ij}^{[p,q]}\middle|\mathbf{a}_a^{[p,q]}\right] = P\left[F_{L,ij}^{[p,q]}|a_a^{(i,j,[p,q])}\right] = \begin{cases} 0 & \text{if } a_a^{(i,j,[p,q])} < a_c^{ij} \\ 1 & \text{if } a_a^{(i,j,[p,q])} \geq a_c^{ij}, \end{cases} \tag{19}$$

and the unconditional modal failure probability is then computed as

$$\begin{aligned} P\left[F_{L,ij}^{[p,q]}\right] &= \int_0^{+\infty} P\left[F_{L,ij}^{[p,q]}|a_a^{(i,j,[p,q])}\right] \times f_{A_a^{(i,j,[p,q])}}\left(a_a^{(i,j,[p,q])}\right) da_a^{(i,j,[p,q])} \\ &= \int_{a_c^{ij}}^{+\infty} f_{A_a^{(i,j,[p,q])}}\left(a_a^{(i,j,[p,q])}\right) da_a^{(i,j,[p,q])} \\ &= 1 - F_{A_a^{(i,j,[p,q])}}\left(a_c^{ij}\right), \end{aligned} \tag{20}$$

where $F_{A_a^{(i,j,[p,q])}}(\cdot)$ represents the CDF of the random variable $A_a^{(i,j,[p,q])}$.

Alternative definitions for the local failure event can be adopted in the proposed framework [15]. For instance, in previous research by Lin et al. [10], Huang and Lin [36], and Backman [37], the local failure event $F_{L,ij}^{[p,q]}$ is defined as $F_{L,ij}^{[p,q]} \triangleq \left\{\left(A_a^{(i,j,[p,q])} \geq a_c^{ij}\right) \cap \left(A_m^{(i,j,[p,q])} < a_c^{ij}\right)\right\}$. This definition, graphically illustrated in Fig. 9, represents the event that the actual damage size, $A_a^{(i,j,[p,q])}$, is greater than the predefined critical damage size (a_c^{ij}), and that the outcome, $A_m^{(i,j,[p,q])}$, from the (assumed) single NDE inspection opportunity at time t_p^q is lower than a_c^{ij}. In this case, the probability of the failure event $F_{L,ij}^{[p,q]}$ conditional on the true damage size $\mathbf{A}_a^{[p,q]} = \mathbf{a}_a^{[p,q]}$ is given by

$$P\left[F_{L,ij}^{[p,q]}|\mathbf{a}_a^{[p,q]}\right] = P\left[F_{L,ij}^{[p,q]}|a_a^{(i,j,[p,q])}\right] = \begin{cases} 0 & \text{if } a_a^{(i,j,[p,q])} < a_c^{ij} \\ 1 - \hat{\psi}\left(a_a^{(i,j,[p,q])}\right) \cdot POD\left(a_a^{(i,j,[p,q])}\right) & \text{if } a_a^{(i,j,[p,q])} \geq a_c^{ij}, \end{cases} \tag{21}$$

where the non-negative function $\hat{\psi}\left(a_a^{(i,j,[p,q])}\right) = \hat{\psi}\left(a_a^{(i,j,[p,q])}; \hat{\beta}_0^{(i,j)}, \hat{\beta}_1^{(i,j)}, \hat{\sigma}_{\varepsilon_{ij}}\right)$ – the derivation of which is provided in Appendix A – is defined as

$$\hat{\psi}\left(a_a^{(i,j,[p,q])}\right) = \Phi\left(\frac{\hat{\beta}_0^{(i,j)} + \hat{\beta}_1^{(i,j)} a_a^{(i,j,[p,q])} - a_c^{ij}}{\hat{\sigma}_{\varepsilon_{ij}}}\right) \times \left[\Phi\left(\frac{\hat{\beta}_0^{(i,j)} + \hat{\beta}_1^{(i,j)} a_a^{(i,j,[p,q])}}{\hat{\sigma}_{\varepsilon_{ij}}}\right)\right]^{-1}. \tag{22}$$

Using the TPT, the unconditional modal failure probability, $P\left[F_{L,ij}^{[p,q]}\right]$, is then computed as

$$\begin{aligned} P\left[F_{L,ij}^{[p,q]}\right] &= \int_0^{+\infty} P\left[F_{L,ij}^{[p,q]}|a_a^{(i,j,[p,q])}\right] \times f_{A_a^{(i,j,[p,q])}}\left(a_a^{(i,j,[p,q])}\right) da_a^{(i,j,[p,q])} \\ &= \left[1 - F_{A_a^{(i,j,[p,q])}}\left(a_c^{ij}\right)\right] - \int_{a_c^{ij}}^{+\infty} \hat{\psi}\left(a_a^{(i,j,[p,q])}\right) \\ &\quad \times POD\left(a_a^{(i,j,[p,q])}\right) f_{A_a^{(i,j,[p,q])}}\left(a_a^{(i,j,[p,q])}\right) da_a^{(i,j,[p,q])}. \end{aligned} \tag{23}$$

Besides the modal probability of failure (computed according to the alternative definition of the local failure event, $F_{L,ij}^{[p,q]}$), it is also of interest to compute the modal probability of false-call (or false-alarm) events for each of the n_A^p local reliability components, with the false-call event defined as $FC_{L,ij}^{[p,q]} \triangleq \left\{\left(A_a^{(i,j,[p,q])} < a_c^{ij}\right) \cap \left(A_m^{(i,j,[p,q])} \geq a_c^{ij}\right)\right\}$ and shown in Fig. 9. The probability of the false-call event $FC_{L,ij}^{[p,q]}$, conditional on the true damage size $\mathbf{A}_a^{[p,q]} = \mathbf{a}_a^{[p,q]}$ (referred herein as conditional modal false-call probability), is given by

$$P\left[FC_{L,ij}^{[p,q]}\middle|\mathbf{a}_a^{[p,q]}\right] = P\left[FC_{L,ij}^{[p,q]}\middle|a_a^{(i,j,[p,q])}\right] = \begin{cases} \hat{\psi}\left(a_a^{(i,j,[p,q])}\right) \cdot POD\left(a_a^{(i,j,[p,q])}\right) & \text{if } a_a^{(i,j,[p,q])} < a_c^{ij} \\ 0 & \text{if } a_a^{(i,j,[p,q])} \geq a_c^{ij}. \end{cases} \tag{24}$$

Using the TPT, the unconditional modal false-call probability, $P\left[FC_{L,ij}^{[p,q]}\right]$, is then computed as

$$\begin{aligned} P\left[FC_{L,ij}^{[p,q]}\right] &= \int_0^{+\infty} P\left[FC_{L,ij}^{[p,q]}|a_a^{(i,j,[p,q])}\right] \times f_{A_a^{(i,j,[p,q])}}\left(a_a^{(i,j,[p,q])}\right) da_a^{(i,j,[p,q])} \\ &= \int_0^{a_c^{ij}} \hat{\psi}\left(a_a^{(i,j,[p,q])}\right) POD\left(a_a^{(i,j,[p,q])}\right) \\ &\quad \times f_{A_a^{(i,j,[p,q])}}\left(a_a^{(i,j,[p,q])}\right) da_a^{(i,j,[p,q])}. \end{aligned} \tag{25}$$

On the other hand, a possible global failure criterion can consider the structural system to have failed when the maximum operational aircraft velocity (V_{MAX}) exceeds either the reduced (due to damage) flutter velocity ($V_F^{[p,q]}$), or any of the n_{LCO} components of the LCO velocity vector ($\mathbf{V}_{LCO}^{[p,q]}$), at time t_p^q [10,11]. Each of the $n_G = 1 + n_{LCO}$ global failure events, with graphical interpretation provided in Fig. 10, is defined as $F_{G,r}^{[p,q]} \triangleq \left\{V_{MAX} \geq V_{F,LCO}^{(r,[p,q])}\right\}$ (with $r = 1, \ldots, n_G$), where the variable V_{MAX} can be characterized probabilistically by the extreme value type I (Gumbel) distribution (Styuart et al., [11]). Furthermore, in this study, V_{MAX} is considered to be s.i. of $\mathbf{V}_{F,LCO}^{[p,q]}$. According to this definition for the global component failure event, $F_{G,r}^{[p,q]}$, the conditional modal failure probabilities can be expressed as

$$P\left[F_{G,r}^{[p,q]}\middle|\mathbf{v}_{F,LCO}^{[p,q]}\right] = P\left[F_{G,r}^{[p,q]}\middle|v_{F,LCO}^{(r,[p,q])}\right] = 1 - F_{V_{MAX}}\left(v_{F,LCO}^{(r,[p,q])}\right), \quad r = 1, \ldots, n_G, \tag{26}$$

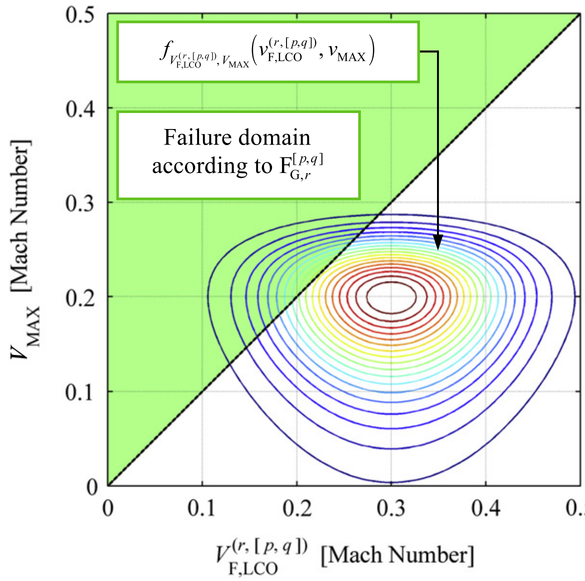

Fig. 10. Failure domain according to the global failure criterion in Eq. (27): V_{MAX} exceeding the rth component of the velocity vector $\mathbf{V}_{F,LCO}^{[p,q]}$, at future time t_p^q, after damage propagation from time t_p to time t_p^q.

and, using the TPT, the corresponding unconditional modal failure probabilities, $P\left[\tilde{F}_{G,r}^{[p,q]}\right]$ (with $r = 1, \ldots, n_G$), are then computed as

$$P\left[F_{G,r}^{[p,q]}\right] = \int_0^{+\infty} P\left[F_{G,r}^{[p,q]} \middle| v_{F,LCO}^{(r,[p,q])}\right] \times f_{V_{F,LCO}^{(r,[p,q])}}\left(v_{F,LCO}^{(r,[p,q])}\right) dv_{F,LCO}^{(r,[p,q])} = 1 - \int_0^{+\infty} F_{V_{MAX}}\left(v_{F,LCO}^{(r,[p,q])}\right) \times f_{V_{F,LCO}^{(r,[p,q])}}\left(v_{F,LCO}^{(r,[p,q])}\right) dv_{F,LCO}^{(r,[p,q])}. \tag{27}$$

Once component reliability analysis has been performed for all, local and global, failure modes, and the corresponding modal failure probabilities have been computed, lower and upper bounds for the probabilities of *system failure* and *false call*, $P\left[F_{sys}^{[p,q]}\right]$ and $P\left[FC_{sys}^{[p,q]}\right]$, can be provided. The system failure event $F_{sys}^{[p,q]}$ is defined as the union of all the n_A^p local and n_G global component failure events described earlier (see Ref. [15]). Lower and upper unimodal bounds for the probability of this failure event are given by Ditlevsen and Madsen [17]:

$$\max_{i,j,r}\left(P\left[F_{L,ij}^{[p,q]}\right], P\left[F_{G,r}^{[p,q]}\right]\right) \leq P\left[F_{sys}^{[p,q]}\right] \leq \min\left(1, \left[\sum_{i=1}^{n_L^{[0,p]}} \sum_{j=1}^{n_{DM}^{(i,[0,p])}} P\left[F_{L,ij}^{[p,q]}\right] + \sum_{r=1}^{n_G} P\left[F_{G,r}^{[p,q]}\right]\right]\right). \tag{28}$$

Furthermore, the structural system is considered failed (conservatively) when the upper bound for $P\left[F_{sys}^{[p,q]}\right]$ reaches or exceeds a critical and predefined safety threshold ($\bar{p}_F$).

Finally, the false-call event for the entire system, $FC_{sys}^{[p,q]}$ (i.e., the event of having a false alarm during an assumed single NDE inspection opportunity at time t_p^q), is defined as

$$FC_{sys}^{[p,q]} \triangleq \left\{\left[\bigcap_{i=1}^{n_L^{[0,p]}} \left(\bigcap_{j=1}^{n_{DM}^{(i,[0,p])}} A_a^{(i,j,[p,q])} < a_c^{ij}\right)\right] \bigcap \left(\bigcap_{i=1}^{n_G} \overline{F_{G,r}^{[p,q]}}\right)\right\} \bigcap \left[\bigcup_{i=1}^{n_L^{[0,p]}} \left(\bigcup_{j=1}^{n_{DM}^{(i,[0,p])}} A_m^{(i,j,[p,q])} \geq a_c^{ij}\right)\right], \tag{29}$$

where $\overline{F_{G,r}^{[p,q]}}$ denotes the complement of the global component failure event $F_{G,r}^{[p,q]}$. Eq. (29) represents the event that, at least for one (i,j) combination, the measured damage size $A_m^{(i,j,[p,q])}$, from the single NDE inspection opportunity at time t_p^q, is larger than or equal to a_c^{ij} and (at the same time) all local and global reliability components, associated with the local and global failure events $F_{L,ij}^{[p,q]}$ and $F_{G,r}^{[p,q]}$, have not failed. Unimodal bounds for $P\left[FC_{sys}^{[p,q]}\right]$ are specified in terms of (i) the modal false-call probabilities, $P\left[FC_{L,ij}^{[p,q]}\right]$ (with $i = 1, \ldots, n_L^{[0,p]}$ and $j = 1, \ldots, n_{DM}^{(i,[0,p])}$), provided in Eq. (25), (ii) the complements of the local component failure probabilities, $F_{A_a^{(i,j,[p,q])}}\left(a_c^{ij}\right)$ (with $i = 1, \ldots, n_L^{[0,p]}$ and $j = 1, \ldots, n_{DM}^{(i,[0,p])}$), derived in Eq. (20), and (iii) the complements of the global component failure probabilities $P\left[\overline{F_{G,r}^{[p,q]}}\right] = 1 - P\left[F_{G,r}^{[p,q]}\right]$ (with $r = 1, \ldots, n_G$). Unimodal lower and upper unimodal bounds for $P\left[FC_{sys}^{[p,q]}\right]$ can be expressed as (see Appendix B)

$$P\left[FC_{sys}^{[p,q]}\right] \geq \max\left(0, P_{low}\left[FC_{local}^{[p,q]}\right] + \sum_{r=1}^{n_G}\left(1 - P\left[F_{G,r}^{[p,q]}\right]\right) - n_G\right) \tag{30}$$

$$P\left[FC_{sys}^{[p,q]}\right] \leq \min\left[P_{up}\left[FC_{local}^{[p,q]}\right], \min_r\left(1 - P\left[F_{G,r}^{[p,q]}\right]\right)\right], \tag{31}$$

where

$$P_{low}\left[FC_{local}^{[p,q]}\right] = \max_{i,j}\left(\frac{P\left[FC_{L,ij}^{[p,q]}\right]}{F_{A_a^{(i,j,[p,q])}}\left(a_c^{ij}\right)}\right) \times \max\left(0, \left[\sum_{i=1}^{n_L^{[0,p]}} \sum_{j=1}^{n_{DM}^{(i,[0,p])}} F_{A_a^{(i,j,[p,q])}}\left(a_c^{ij}\right)\right] - \left(n_A^p - 1\right)\right) \tag{32}$$

and

$$P_{up}\left[FC_{local}^{[p,q]}\right] = \min\left(1, \left[\sum_{i=1}^{n_L^{[0,p]}} \sum_{j=1}^{n_{DM}^{(i,[0,p])}} \frac{P\left[FC_{L,ij}^{[p,q]}\right]}{F_{A_a^{(i,j,[p,q])}}\left(a_c^{ij}\right)}\right]\right) \times \min_{i,j}\left[F_{A_a^{(i,j,[p,q])}}\left(a_c^{ij}\right)\right]. \tag{33}$$

8. Conclusions

A comprehensive reliability-based methodology for predicting the remaining service life of composite aircraft structures (with emphasis on a composite wing structure) has been presented. These structures are fabricated using high-performance lightweight composite materials with outstanding in-plane (fiber dominated) strengths but very low out-of-plane and adhesive strengths, a weakness fostering the initiation of damage mechanisms (e.g., debonding, inter-ply delamination, etc.) which can then rapidly propagate up to catastrophic levels (i.e., in-flight aircraft failure). In this study, it is assumed that the damage propagation process is purely fatigue driven (even though impact-induced damage could also be integrated in the proposed methodology). The prognosis framework presented in this research relies on (i) in-flight (through a built-in sensor network) and on-ground NDE inspections to probabilistically assess and recursively update the current state of damage of the monitored structural component, and (ii) stochastic prediction of the evolution in time of the detected damage mechanisms at multiple damage locations through calibrated and validated computationally efficient metamodeling approaches. Probabilistic damage evolution analysis and probabilistic flutter and LCO analyses are used in the proposed methodology to provide estimates of the joint PDF of the local and global states of damage at the generic future time $t_p^q = t_p + q \cdot \Delta\tau$ (where t_p denotes the time of the last NDE inspection and $\Delta\tau$ is a fixed time interval between two successive damage prognosis predictions). This probabilistic information of the overall state of damage is then used, through state-of-the-art component and system reliability analysis methods, to compute lower and upper bounds for the probability of *system failure*, $P\left[F_{\text{sys}}^{[p,q]}\right]$, accounting for both local (structural) and global (aeroelastic) failure modes. Finally, the estimates of $P\left[F_{\text{sys}}^{[p,q]}\right]$ at future times t_p^q (with $q = 1, 2, \ldots, \bar{q}$) can then be used as rational decision-making parameters/variables to schedule and/or update the maintenance/repair plan on the basis of a predefined maximum acceptable threshold ($\bar{p}_{\text{F}}$) for $P\left[F_{\text{sys}}^{[p,q]}\right]$.

The proposed methodology thus represents an advanced tool for fatigue damage prognosis of a composite wing structure by integrating NDE inspection, Bayesian inference, stochastic characterization, and superposition of turbulence-induced and maneuver-induced aerodynamic loads, mechanics-based damage evolution prediction and its surrogate modeling for uncertainty propagation, and decision making. However, it can be extended to the entire airframe, or more generally to any structural system with potential multi-site fatigue-driven and/or corrosion-driven damage growth, monitored (nearly continuously or periodically) through NDE inspections during its service life. Potential fields of applicability include the following: mechanical systems, such as wind turbines; civil infrastructures, such as FRP-retrofitted concrete bridges, offshore platforms, nuclear facilities, and water dams; automotive and naval systems; and military infrastructure and equipment, such as lightweight deployable bridges. The proposed probabilistic damage prognosis framework can also be used to assess the time-varying reliability of aging structures and infrastructures and develop a sustainable, reliability-based, cost-efficient management and maintenance program. Finally, the work presented herein constitutes the fundamental basis for forthcoming additional theoretical developments, numerical applications, validations, and extension to other engineering fields.

Acknowledgments

The work presented in this paper is part of a research project funded by the Educational Collaboration between the Los Alamos National Laboratory (LANL) and the University of California, San Diego, (UCSD) on "A Damage Prognosis System for Unmanned Aerial Vehicles"; contract number: 72232-001-03. Partial support for the work presented was also provided by the UCSD Academic Senate Research Grant RJ086G-CONTE. The authors wish to thank Dr. Gyuhae Park and Dr. François Hemez of the Los Alamos National Laboratory for valuable technical discussions on the subject of this study.

Appendix A. Derivation of equations (21) and (22)

For a given value of the actual damage size $A_a^{(i,j,[p,q])} = a_a^{(i,j,[p,q])}$, and in the range $a_a^{(i,j,[p,q])} \geq a_c^{ij}$, the conditional modal probability of failure, $P\left[F_{\text{L},ij}^{[p,q]} \middle| a_a^{(i,j,[p,q])}\right]$, with the failure event $F_{\text{L},ij}^{[p,q]}$ defined as $F_{\text{L},ij}^{[p,q]} \triangleq \{(A_a^{(i,j,[p,q])} \geq a_c^{ij}) \cap (A_m^{(i,j,[p,q])} < a_c^{ij})\}$, can be written as

$$\begin{aligned} P\left[F_{\text{L},ij}^{[p,q]} \middle| a_a^{(i,j,[p,q])}\right] &= P\left[\left\{\left(A_a^{(i,j,[p,q])} \geq a_c^{ij}\right) \bigcap \left(A_m^{(i,j,[p,q])} < a_c^{ij}\right)\right\} \middle| a_a^{(i,j,[p,q])}\right] \\ &= P\left[A_m^{(i,j,[p,q])} < a_c^{ij} \middle| a_a^{(i,j,[p,q])}\right]. \end{aligned} \tag{A.1}$$

Using the TPT and the definition of *POD* given in Eq. (5) in Section 3, Eq. (A.1) can be rewritten as

$$\begin{aligned} P\left[F_{\text{L},ij}^{[p,q]} | a_a^{(i,j,[p,q])}\right] &= P\left[A_m^{(i,j,[p,q])} < a_c^{ij} \middle| a_a^{(i,j,[p,q])}, D\right] POD\left(a_a^{(i,j,[p,q])}\right) \\ &\quad + P\left[A_m^{(i,j,[p,q])} < a_c^{ij} \middle| a_a^{(i,j,[p,q])}, ND\right]\left[1 - POD\left(a_a^{(i,j,[p,q])}\right)\right] \\ &= P\left[A_m^{(i,j,[p,q])} < a_c^{ij} \middle| a_a^{(i,j,[p,q])}, D\right] POD\left(a_a^{(i,j,[p,q])}\right) \\ &\quad + \left[1 - POD\left(a_a^{(i,j,[p,q])}\right)\right], \end{aligned} \tag{A.2}$$

where D represents the detection event defined as $D \triangleq \left\{A_m^{(i,j,[p,q])} > 0\right\}$ and ND denotes its complement (i.e., the non-detection event) defined as $ND \triangleq \left\{A_m^{(i,j,[p,q])} = 0\right\}$. Using Eq. (10) to express the probability $P\left[A_m^{(i,j,[p,q])} < a_c^{ij} \middle| a_a^{(i,j,[p,q])}, D\right]$, the above equation further simplifies to

$$\begin{aligned} P\left[F_{\text{L},ij}^{[p,q]} \middle| a_a^{(i,j,[p,q])}\right] &= 1 - \left[1 - \left(\int_{0^+}^{a_c^{ij}} \tilde{\varphi}\left(a_m^{(i,j,[p,q])}, \hat{\mu}_{A_m|A_a}^{(i,j,[p,q])}, \hat{\sigma}_{\varepsilon_{ij}}\right) da_m^{(i,j,[p,q])}\right)\right] \\ &\quad \times POD\left(a_a^{(i,j,[p,q])}\right), \end{aligned} \tag{A.3}$$

where the integral between 0^+ and a_c^{ij} of the function $\tilde{\varphi}\big(a_m^{(i,j,[p,q])}; \hat{\mu}_{A_m|A_a}^{(i,j,[p,q])}, \hat{\sigma}_{\varepsilon_{ij}}\big)$ is given by

$$\begin{aligned} &\int_{0^+}^{a_c^{ij}} \tilde{\varphi}\left(a_m^{(i,j,[p,q])}, \hat{\mu}_{A_m|A_a}^{(i,j,[p,q])}, \hat{\sigma}_{\varepsilon_{ij}}\right) da_m^{(i,j,[p,q])} \\ &\quad = \frac{\Phi\left(\frac{a_c^{ij} - \hat{\mu}_{A_m|A_a}^{(i,j,[p,q])}}{\hat{\sigma}_{\varepsilon_{ij}}}\right) - \Phi\left(-\frac{\hat{\mu}_{A_m|A_a}^{(i,j,[p,q])}}{\hat{\sigma}_{\varepsilon_{ij}}}\right)}{\Phi\left(\frac{\hat{\mu}_{A_m|A_a}^{(i,j,[p,q])}}{\hat{\sigma}_{\varepsilon_{ij}}}\right)} \\ &\quad = 1 - \frac{\Phi\left(\frac{\hat{\mu}_{A_m|A_a}^{(i,j,[p,q])} - a_c^{ij}}{\hat{\sigma}_{\varepsilon_{ij}}}\right)}{\Phi\left(\frac{\hat{\mu}_{A_m|A_a}^{(i,j,[p,q])}}{\hat{\sigma}_{\varepsilon_{ij}}}\right)} \\ &\quad = 1 - \frac{\Phi\left(\frac{\hat{\beta}_0^{(i,j)} + \hat{\beta}_1^{(i,j)} a_a^{(i,j,[p,q])} - a_c^{ij}}{\hat{\sigma}_{\varepsilon_{ij}}}\right)}{\Phi\left(\frac{\hat{\beta}_0^{(i,j)} + \hat{\beta}_1^{(i,j)} a_a^{(i,j,[p,q])}}{\hat{\sigma}_{\varepsilon_{ij}}}\right)} \\ &\quad = 1 - \hat{\psi}\left(a_a^{(i,j,[p,q])}; \hat{\beta}_0^{(i,j)}, \hat{\beta}_1^{(i,j)}, \hat{\sigma}_{\varepsilon_{ij}}\right). \end{aligned} \tag{A.4}$$

Lastly, by substituting the final result from Eq. (A.4) in Eq. (A.3), the conditional modal probability of failure, $P\left[F_{\text{L},ij}^{[p,q]} \middle| a_a^{(i,j,[p,q])}\right]$ (with $a_a^{(i,j,[p,q])} \geq a_c^{ij}$), can be expressed as

$$\begin{aligned} P\left[F_{\text{L},ij}^{[p,q]} | a_a^{(i,j,[p,q])}\right] &= 1 - \hat{\psi}\left(a_a^{(i,j,[p,q])}; \hat{\beta}_0^{(i,j)}, \hat{\beta}_1^{(i,j)}, \hat{\sigma}_{\varepsilon_{ij}}\right) \\ &\quad \times POD\left(a_a^{(i,j,[p,q])}\right). \end{aligned} \tag{A.5}$$

Appendix B. Derivation of lower and upper unimodal bounds for the probability of the false-call event $FC_{\text{sys}}^{[p,q]}$

The logical expression for the false-call event $FC_{\text{sys}}^{[p,q]}$, provided in Eq. (29), clearly represents a combination of series and parallel systems, and can be rearranged as

$$
\begin{aligned}
FC_{\text{sys}}^{[p,q]} \triangleq & \left\{ \left[\bigcap_{i=1}^{n_{\text{L}}^{[0,p]}} \left(\bigcap_{j=1}^{n_{\text{DM}}^{(i,[0,p])}} A_a^{(i,j,[p,q])} < a_c^{ij} \right) \right] \bigcap \left(\bigcap_{i=1}^{n_{\text{G}}} \overline{F_{\text{G},r}^{[p,q]}} \right) \right\} \\
& \bigcap \left[\bigcup_{i=1}^{n_{\text{L}}^{[0,p]}} \left(\bigcup_{j=1}^{n_{\text{DM}}^{(i,[0,p])}} A_m^{(i,j,[p,q])} \geq a_c^{ij} \right) \right] \\
& \triangleq FC_{\text{local}}^{[p,q]} \bigcap \left(\bigcap_{i=1}^{n_{\text{G}}} \overline{F_{\text{G},r}^{[p,q]}} \right), \qquad \text{(B.1)}
\end{aligned}
$$

where the event $FC_{\text{local}}^{[p,q]}$ would represent the false-call event (at the overall system level) when only the local reliability components (or local failure modes) are considered. The probability of this event, herein denoted by $P\left[FC_{\text{local}}^{[p,q]}\right]$, can be computed as

$$
\begin{aligned}
P\left[FC_{\text{local}}^{[p,q]}\right] = & P\left[\left\{ \bigcup_{i=1}^{n_{\text{L}}^{[0,p]}} \left(\bigcup_{j=1}^{n_{\text{DM}}^{(i,[0,p])}} A_m^{(i,j,[p,q])} \geq a_c^{ij} \right) \right\} \right| \\
& \left. \left\{ \bigcap_{i=1}^{n_{\text{L}}^{[0,p]}} \left(\bigcap_{j=1}^{n_{\text{DM}}^{(i,[0,p])}} A_a^{(i,j,[p,q])} < a_c^{ij} \right) \right\} \right] \\
& \times P\left[\left\{ \bigcap_{i=1}^{n_{\text{L}}^{[0,p]}} \left(\bigcap_{j=1}^{n_{\text{DM}}^{(i,[0,p])}} A_a^{(i,j,[p,q])} < a_c^{ij} \right) \right\} \right] \\
= & P[E_1|E_2] \times P[E_2], \qquad \text{(B.2)}
\end{aligned}
$$

where the two events E_1 and E_2 are introduced for the sake of conciseness. Event E_1 in Eq. (B.2) can be viewed as the failure event of a series system with $n_{\text{A}}^p = \sum_{i=1}^{n_{\text{L}}^{[0,p]}} n_{\text{DM}}^{(i,[0,p])}$ components. Thus, similarly to Eq. (28), lower and upper unimodal bounds for $P[E_1|E_2]$ can be obtained (see Eqs. (B.3) and (B.4)) by making use of assumption (iii) about the damage size measurement model used herein (see Section 3) and the definition of the false-call event $FC_{\text{L},ij}^{[p,q]} \triangleq \left\{ \left(A_a^{(i,j,[p,q])} < a_c^{ij} \right) \cap \left(A_m^{(i,j,[p,q])} \geq a_c^{ij} \right) \right\}$.

$$
\begin{aligned}
P[E_1|E_2] & \geq \max_{i,j} \left(P\left[A_m^{(i,j,[p,q])} \geq a_c^{ij} \, | E_2 \right] \right) \\
& \geq \max_{i,j} \left(P\left[A_m^{(i,j,[p,q])} \geq a_c^{ij} \, \middle| A_a^{(i,j,[p,q])} < a_c^{ij} \right] \right) \\
& \geq \max_{i,j} \left(\frac{P\left[FC_{\text{L},ij}^{[p,q]}\right]}{F_{A_a^{(i,j,[p,q])}}\left(a_c^{ij}\right)} \right) \qquad \text{(B.3)}
\end{aligned}
$$

$$
\begin{aligned}
& P[E_1|E_2] \\
& \leq \min\left(1, \left[\sum_{i=1}^{n_{\text{L}}^{[0,p]}} \sum_{j=1}^{n_{\text{DM}}^{(i,[0,p])}} P\left[A_m^{(i,j,[p,q])} \geq a_c^{ij} \, | E_2 \right] \right] \right) \\
& \leq \min\left(1, \left[\sum_{i=1}^{n_{\text{L}}^{[0,p]}} \sum_{j=1}^{n_{\text{DM}}^{(i,[0,p])}} P\left[A_m^{(i,j,[p,q])} \geq a_c^{ij} \, \middle| \, A_a^{(i,j,[p,q])} < a_c^{ij} \right] \right] \right) \\
& \leq \min\left(1, \left[\sum_{i=1}^{n_{\text{L}}^{[0,p]}} \sum_{j=1}^{n_{\text{DM}}^{(i,[0,p])}} \frac{P\left[FC_{\text{L},ij}^{[p,q]}\right]}{F_{A_a^{(i,j,[p,q])}}\left(a_c^{ij}\right)} \right] \right). \qquad \text{(B.4)}
\end{aligned}
$$

The second term on the right-hand side of Eq. (B.2) – i.e., $P[E_2]$ – can be viewed as a parallel system for which the narrowest lower and upper unimodal bounds [38] are expressed as

$$
\begin{aligned}
& \max\left(0, \left[\sum_{i=1}^{n_{\text{L}}^{[0,p]}} \sum_{j=1}^{n_{\text{DM}}^{(i,[0,p])}} F_{A_a^{(i,j,[p,q])}}\left(a_c^{ij}\right) \right] - \left(n_{\text{A}}^P - 1\right) \right) \\
& \leq P[E_2] \leq \min_{i,j} \left(F_{A_a^{(i,j,[p,q])}}\left(a_c^{ij}\right) \right). \qquad \text{(B.5)}
\end{aligned}
$$

Then, substituting the results of Eqs. (B.3)–(B.5) in Eq. (B.2) (multiplying lower bound with lower bound and upper bound with upper bound) yields the lower and upper unimodal bounds of $P\left[FC_{\text{local}}^{[p,q]}\right]$ provided in Eqs. (32) and (33). Finally, the lower and upper unimodal bounds for the parallel system defined as $FC_{\text{sys}}^{[p,q]} \triangleq FC_{\text{local}}^{[p,q]} \cap \left(\cap_{r=1}^{n_{\text{G}}} \overline{F_{\text{G},r}^{[p,q]}} \right)$ are computed, according to Ref. [38]. This approach leads to the final results shown in Eqs. (30) and (31).

References

[1] Yang JN, Trapp WJ. Reliability analysis of aircraft structures under random loading and periodic inspection. AIAA Journal 1974;12(12):1623–30.

[2] Deodatis G, Asada H, Ito S. Reliability of aircraft structures under non-periodic inspection: a Bayesian approach. Engineering Fracture Mechanics 1996;53(5): 789–805.

[3] Lin KY, Styuart AV. Probabilistic approach to damage tolerance design of aircraft composite structures. Journal of Aircraft 2007;44(4):1309–17.

[4] Oliver JA, Kosmatka JB, Farrar CR, Park Gyuhae. Development of a composite UAV wing test-bed for structural health monitoring research. In: Proceedings of SPIE Smart Structures and Materials & Nondestructive Evaluation and Health Monitoring; 2007.

[5] Bauchau OA, Loewy RG. Nonlinear aeroelastic effects in damaged composite aerospace structures. Technical report, School of Aerospace Engineering. Georgia Institute of Technology, Atlanta. GA, 1997.

[6] Wang K, Inman DJ, Farrar CR. Crack-induced changes in divergence and flutter of cantilevered composite panels. Structural Health Monitoring 2005;4(4): 377–92.

[7] Inman DJ, Farrar CR, Lopez Jr V, Steffen Jr V. Damage prognosis for aerospace, civil and mechanical systems. West Sussex, England: John Wiley and Sons; 2005.

[8] Moehle J, Deierlein GG. A framework methodology for performance-based earthquake engineering. In: Proceedings of 13th conference on earthquake engineering; 2004.

[9] Lanza di Scalea F, Matt HM, Bartoli I, Coccia S, Park G, Farrar CR. Health monitoring of UAV skin-to-spar joints using guided waves and macro fiber composite transducers. Journal of Intelligent Material Systems and Structures 2007;18(4):373–88.

[10] Lin KY, Du J, Rusk D. Structural design methodology based on concepts of uncertainty. In: NASA/CR-2000-209847. Hampton, VA: NASA Langley Research Center; 2000.

[11] Styuart AV, Mor M, Livne E, Lin KY. Aeroelastic failure risk assessment in damage tolerant composite airframe structures. In: Proceedings of 48th AIAA/ASME/ASCE/AHS/ASC structures, structural dynamics, and materials conference; 2007.

[12] Paris PC, Erdogan FA. Critical analysis of crack propagation laws. Journal of Basic Engineering, TRANS ASME 1963;85(Series D):528–34.

[13] Degrieck J, Paepegem WV. Fatigue damage modeling of fibre-reinforced composite materials: review. Applied Mechanics Reviews 2001;54(4):279–99.

[14] Alfano G, Crisfield MA. Finite element interface models for the delamination analysis of laminated composites: mechanical and computational issues. International Journal for Numerical Methods in Engineering 2001;50(7): 1701–36.

[15] Gobbato M, Conte JP, Kosmatka JB, Farrar CR. Reliability-based damage prognosis framework for bonded joints in composite unmanned aircrafts. Report No. SSRP-11/03. Department of Structural Engineering. University of California, San Diego, 2011.

[16] Myers RH, Montgomery DC. Response surface methodology. New York, NY: John Wiley and Sons, Inc; 1995.

[17] Ditlevsen O, Madsen HO. Structural reliability methods. West Sussex, England: John Wiley and Sons; 1996.

[18] Silk MG, Stoneham AM, Temple JAG. The reliability of nondestructive inspection. Institute of Physics Publishing; 1987.

[19] Berens AP. NDE reliability analysis. 9th ed. Metals handbook, vol. 17. ASM International; 1989. p. 689–701.

[20] Staat M. Sensitivity of and influences on the reliability of an HTR-module primary circuit pressure boundary. In: Proceedings of 12th international conference on structural mechanics in reactor technology (SMiRT); 1993.

[21] Zhang R, Mahadevan S. Fatigue reliability analysis using non-destructive inspection. Journal of Structural Engineering 2001;127(8):957–65.
[22] Zheng R, Ellingwood BR. Role of non-destructive evaluation in time-dependent reliability analysis. Structural Safety 1998;20(4):325–39.
[23] Kulkarni SS, Achenbach JD. Structural health monitoring and damage prognosis in fatigue. Structural Health Monitoring 2008;7(1):37–49.
[24] Hoblit FM. Gust loads on aircraft: concepts and applications, AIAA Ed. Series. Washington, D.C; 1988.
[25] Van Staveren WH. Analyses of aircraft responses to atmospheric turbulence. Ph.D. Dissertation. The Netherlands: Department of Aerospace Design, Integration & Operations. Delft University of Technology; 2003.
[26] Kordes EE, Love BJ. Preliminary evaluation of XB-70 airplane encounters with high-altitude turbulence. Edwards, California, NASA: NASA Flight Research Center; 1967. TN D-4209.
[27] Coleman TL, Steiner R. Atmospheric turbulence measurements obtained from airplanes operations at altitudes between 20,000 and 75,000 feet for several areas in the northern hemisphere. Hampton, Virginia, NASA: NASA Langley Research Center; 1960. TN D-548.
[28] Rustenburg JW, Skinn D, Tipps DO. An evaluation of methods to separate maneuver and gust load factors from measured acceleration time histories, US Department of Transportation. Federal Aviation Administration. Report No. DOT/FAA/AR-99/14, 1999.
[29] Rustenburg JW, Skinn D, Tipps DO. Development of an improved maneuver-gust separation criterion. University of Dayton Research Institute (UDRI), Structural Integrity Division; 2008.
[30] Rustenburg JW, Skinn D, Tipps DO. Statistical loads data for Boeing 737–400 aircraft in commercial operations. US Department of Transportation, Federal Aviation Administration; 1998.
[31] Wen Y-K. Structural load modeling and combination for performance and safety evaluation. Elsevier; 1990.
[32] McFarland JM. Uncertainty analysis for computer simulations through validation and calibration. Ph.D. Thesis. Nashville. TN: Department of Mechanical Engineering, Vanderbilt University; 2008.
[33] Sanford RJ. Principles of fracture mechanics. Prentice Hall; 2003.
[34] Navarro A, De Los Rios ER. On dimensional analysis of fatigue crack growth rate and geometrical similitude of cracks. Fatigue & Fracture of Engineering Materials and Structures 1987;9(5):373–8.
[35] Safi SA, Kelly DW, Archer RD. Interaction between wear processes and limit cycle oscillations of a control surface with free-play nonlinearity. Proceedings of Institution of Mechanical Engineers, Part G: Journal of Aerospace Engineering 2002;216(3):143–53.
[36] Huang C, Lin KY. A method for reliability assessment of aircraft structures subject to accidental damage. In: Proc. 46th AIAA/ASME/ASCE/AHS/ASC structures, structural dynamics, & materials conference; 2005.
[37] Backman BF. Composite structures, design, safety and innovation. Elsevier; 2005.
[38] Fréchet M. Généralisations du théorème des probabilités totales. Fundamenta Mathematicae 1935;25:379–87.